
ROBUST AND FAST BASS LOCAL VOLATILITY

Hao Qin[†],  Charlie Che^{†‡}, Ruozhong Yang[†], and Liming Feng^{†*}

[†]Department of Industrial and Enterprise Systems Engineering, University of Illinois Urbana-Champaign, Illinois, United States

[‡]JPMorgan Chase & Co., New York, United States

ABSTRACT

The Bass Local Volatility Model, as studied in [Conze and Henry-Labordere, 2021], stands out for its ability to eliminate the need for interpolation between maturities. This offers a significant advantage over traditional local volatility models. However, its performance highly depends on accurate construction of risk neutral densities and the corresponding marginal distributions and efficient numerical convolutions which are necessary when solving the associated fixed point problems. In this paper, we propose a new approach combining local quadratic estimation and lognormal mixture tails for the construction of risk neutral densities. We investigate computational efficiency of trapezoidal rule based schemes for numerical convolutions and show that they outperform commonly used Gauss-Hermite quadrature. We demonstrate the performance of the proposed method, both in standard option pricing models, as well as through a detailed market case study.

Keywords: Bass Local Volatility, risk neutral density, local quadratic estimation, lognormal mixture tails, numerical integration, trapezoidal rule

Key Messages:

- Development of high quality arbitrage-free risk neutral densities necessary for Bass local volatility implementation
- Theoretical and numerical evidence of the trapezoidal rule's superiority over Gauss-Hermite quadrature for numerical convolution in the Bass local volatility implementation

1 Introduction

In derivatives pricing, local volatility (LV) models have been widely adopted, particularly in applications involving the valuation of exotic options [Dupire et al., 1994][Derman et al., 1996][Coleman et al., 2001][Bouzoubaa and Osseiran, 2010][Kotzé et al., 2015]. Dupire's formulation of LV models provides a deterministic framework where instantaneous volatility is a function of both the asset price and time. Since Dupire's seminal work, this framework has become a key tool and industry standard for characterizing the dynamics of underlying asset prices. However, practical application of such models faces challenges due to the lack of observable vanilla option prices across all strikes and maturities. One of the main challenges is the need for an arbitrage-free interpolation scheme for volatilities at unobserved maturities. The time interpolation and related extrapolation can introduce instabilities and make the model highly sensitive to variations in market data.

This difficulty can be effectively addressed by the Bass-LV construction proposed by [Conze and Henry-Labordere, 2021]. The Bass-LV construction, rooted in the Bass martingale, is a solution to the Martingale Benamou-Brenier problem introduced by [Backhoff et al., 2017]. The Bass-LV model leverages the martingale property of the asset price process to ensure the absence of calendar arbitrage, thereby circumventing the need for direct time interpolation of volatilities. This construction is particularly advantageous because it aligns with the martingale condition, which is a fundamental requirement for no-arbitrage pricing in derivatives markets.

*Corresponding author. Email: fenglm@illinois.edu

The Bass-LV model is particularly well-suited for pricing a wide array of exotic payoffs, such as autocalls, forward-start options, lookback options, and Asian options. Its accuracy and flexibility in addressing the complex and diverse needs of exotic option pricing make Bass-LV a competitive choice in volatility modeling. The model takes implied risk neutral densities as inputs and calibrates the spot price process by solving a fixed-point problem numerically. The calibrated spot price process is trivial to simulate. Monte Carlo methods can then be easily used to evaluate any financial option contract.

Recent theoretical work by [Acciaio et al., 2023] further advances the Bass-LV theory, demonstrating a linear convergence rate of the numerical scheme in the fixed-point algorithm. [Tschiderer, 2024] extends the Bass-LV construction by replacing the Gaussian transition kernel with an arbitrary reference measure, which provides more flexibility in fitting different financial assets. [Loeper, 2023] introduces additional PDE methods for computing the fixed-point iterations, which offer an alternative approach to the calibration process. Moreover, [Backhoff-Veraguas et al., 2023a] and [Backhoff-Veraguas et al., 2023b] give general theoretical results by analyzing the dual formulation of the Bass martingale, and strengthen the model's theoretical foundation.

The concept of leveraging martingales in Bass-LV is indeed a part of Martingale Optimal Transport (MOT), which extends the classical Optimal Transport problem [Monge, 1781] by incorporating the martingale property. Beyond the Bass-LV construction, a variety of research has explored alternative MOT frameworks to address different problem settings. For example, [Henry-Labordere, 2019a] gives a new class of stochastic volatility models by combining martingale Schrödinger bridges with the Sinkhorn algorithm from [De March and Henry-Labordere, 2019]. [Eckstein and Kupper, 2021] gives a feed-forward neural network formulation of MOT problems that enables a neural network solution for problems constructed in high dimensional space with multiple assets. [Henry-Labordere, 2019b] proposes a primal-dual algorithm for solving MOT problems that leverages the capabilities of generative adversarial networks. Some other related works can be seen in [Hobson and Neuberger, 2012], [Beiglböck et al., 2013], [Dolinsky and Soner, 2014], [Henry-Labordere and Touzi, 2016], [Guo et al., 2017], [Henry-Labordere, 2017], and [Nutz et al., 2023].

Despite its advantages over traditional LV models, the Bass-LV model still exhibits certain limitations, particularly in its numerical implementation. First, the model relies on a fixed-point algorithm that involves multiple convolutions, often implemented using the Gauss-Hermite quadrature. Preliminary results suggest that using a small number of quadrature points often compromises accuracy, while raising the number significantly increases computational time. Second, computing implied risk neutral densities and the corresponding marginal distributions of the underlying asset price commonly depends on simple interpolation and extrapolation based on the Breeden-Litzenberger formula. However, such techniques cannot be directly applied due to arbitrage present in market data. Even after removing arbitrage, calibration stability cannot be guaranteed due to insufficient modeling of the tails of the distributions.

These limitations highlight the need for new approaches for the calibration of the Bass-LV model. Our research aims to address these challenges by proposing robust and fast numerical schemes and methods that enhance both the stability and accuracy of the Bass-LV model in practical applications.

In the following, Section 2 provides a review of the mathematical background related to Bass-LV construction. Section 3 leverages a local quadratic regression model with adaptive parameters to generate the arbitrage-free risk neutral density from observable option prices. A lognormal mixture is used for tails approximation of the density. Section 4 analyzes the optimal parameter selection and convergence of the trapezoidal rule for numerical convolution. It is then compared to the Gauss-Hermite quadrature scheme. Section 5 starts with a Black-Scholes example to illustrate the relationship between the iteration tolerance level for the fixed-point problem and calibration accuracy of the Bass-LV model. This is followed by a comparison between our proposed method and the classical Breeden-Litzenberger formulation within the Heston-like Stochastic-Volatility-Inspired (SSVI) model. Finally, a market case study is conducted to demonstrate the practical applicability of the proposed method.

2 Bass-LV

The Bass-LV model stands out as a Markov model that achieves precise calibration to the underlying asset price distributions μ_1, \dots, μ_n implied from market prices of European vanilla options across a range of maturities $T_0 = 0 \leq T_1 < \dots < T_n = T$. The core of the Bass-LV model lies in the extension of the Bass martingale construction within the context of the Skorokhod embedding problem. To be specific, given probability distributions $\mu_1 < \dots < \mu_n$ in $\mathcal{P}(\mathbb{R})$ that are ordered in convex sense, the objective is to construct a martingale M_t such that $M_t = f_t(W_t, t)$, $t \in [T_i, T_{i+1}]$, $M_{T_i} \sim \mu_i$, and $M_{T_{i+1}} \sim \mu_{i+1}$. Here, $\mathcal{P}(\mathbb{R})$ denotes the collection of all probability measures defined on the real line \mathbb{R} , and W_t denotes a predictable RCLL process (right-continuous with left limits) such that $W_t = W_{T_i} + B_t - B_{T_i}$ for all $t \in [T_i, T_{i+1}]$ and for all $i = 0, \dots, n-1$, with $(B_t)_{0 \leq t \leq T}$ being a standard Brownian motion. Notice that the generalization of the Bass-LV from the classical Bass Martingale is indeed not trivial. For the classical Bass Martingale in the one-dimensional case, the initial marginal distribution is a Dirac measure δ_m , where m is the mean

of some random variable ν . It turns out the solution to the martingale optimal transport problem (also known as stretched Brownian Motion) is equivalent to finding the martingale that closely tracks a baseline Brownian motion while respecting the initial and terminal marginals. As such, finding the solution comes down to finding a monotone increasing function $f : \mathbb{R} \mapsto \mathbb{R}$ such that $f(\gamma) = \nu$ where γ is a standard normal random variable on \mathbb{R} . The martingale M_t can be defined as

$$M_t := \mathbb{E}[f(B_1)|\mathcal{F}] = \mathbb{E}[f(B_1)|B_t] = f_t(B_t). \quad (1)$$

This turns out to be trivial to construct. At the terminal, i.e. where f maps from B_1 to ν , f is simply the Frechet Hoeffding solution $f = F_\nu^{-1} \circ F_{B_1} = F_\nu^{-1} \circ \mathcal{N}(\sigma)$ where F and F^{-1} denote the CDF and the inverse CDF of the respective distribution. Given that the lifted space is a Martingale, f must obey the heat equation. In this vein, defining f on all of $t \in [0, 1]$ boils down to solving the heat equation with terminal condition defined by the Frechet Hoeffding solution. From classical PDE theory, this is simply the convolution of the terminal condition with the heat kernel operator:

$$\frac{\partial f}{\partial t} + \frac{1}{2} \frac{\partial^2 f}{\partial \sigma^2} f = 0, \quad (2)$$

$$f(\sigma, 1) = F_\nu^{-1} \circ F_{B_1}, \quad (3)$$

$$f(\sigma, t) = \mathcal{K}_{1-t} * f(\sigma, 1) = \mathcal{K}_{1-t} * (F_\nu^{-1} \circ F_{B_1}). \quad (4)$$

In general, when the initial marginal μ is not trivial, the base process cannot be assumed to be reversible. Therefore, finding the optimizer for the Martingale Benamou Brenier problem is equivalent to finding the initial marginal for the base process. Specifically, in the Bass local volatility case, the LV calibration reduces to devising a fixed point algorithm as in [Conze and Henry-Labordere, 2021] to find the initial base distribution of α . Figure 1 illustrates the Bass martingale, where similar idea can be seen in [Acciaio et al., 2023]; and Figure 2 shows the main idea of Bass-LV.

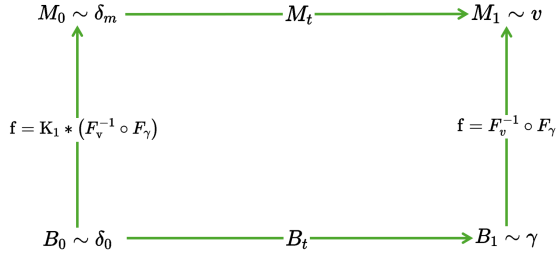


Figure 1: Bass Martingale

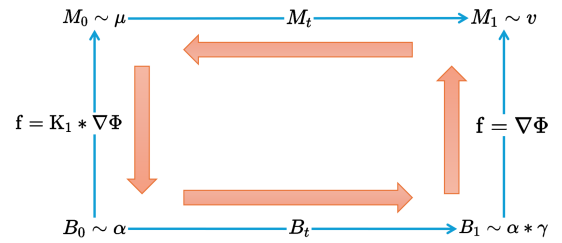


Figure 2: Bass Local Volatility

The function $f_t(x) : [T_i, T_{i+1}] \times \mathbb{R} \rightarrow \mathbb{R}$ defines the underlying spot price process S_t between two given maturities.

To calibrate the specific W_t for $t \in [T_i, T_{i+1}]$, one needs to apply a fixed-point algorithm for the cumulative distribution function (CDF) of W_t : $F_{W_{T_i}} = \mathcal{A}F_{W_{T_i}}$, where \mathcal{A} is a nonlinear operator given by

$$\mathcal{A}F := F_{\mu_i} \circ \left(K_{T_{i+1}-T_i} * \left(F_{\mu_{i+1}}^{-1} \circ \left(K_{T_{i+1}-T_i} * F \right) \right) \right).$$

Here, K is the heat kernel $K_t(x) := \frac{e^{-\frac{x^2}{2t}}}{\sqrt{2\pi t}}$, \circ denotes the composition operator, and $*$ the convolution.

In numerical practice, we start the calibration with an initial guess of Gaussian distribution for that specific random process W_t . The spot price process can then be expressed by $f(t, \cdot) = K_{T_{i+1}-t} * \left(F_{\mu_{i+1}}^{-1} \circ \left(K_{T_{i+1}-T_i} * F_{W_{T_i}} \right) \right)$, where $F_{W_{T_i}}$ is the numerical solution of the fixed-point problem. Monte Carlo methods can then be used to price any financial option of interest by simulating the spot price process f .

3 Construction of Arbitrage-Free Risk Neutral Densities

In this section, we give details of the proposed method for obtaining arbitrage-free risk neutral density from options data. The densities are then used to generate the marginal distributions required for the construction of the Bass-LV model. We focus on formulations based on vanilla call options. Formulations based on put options can be obtained similarly.

Consider the European call option pricing formula from the Black-Scholes model:

$$C_t(K, \tau) = S_t \Phi(d_1(K)) - K e^{-r\tau} \Phi(d_2(K)),$$

where S_t is the underlying asset price at time t , K is the strike price, r is the risk-free interest rate, $\tau = T - t$ is the time-to-maturity, and σ is the volatility of the asset. The terms d_1 and d_2 are given by:

$$d_1(K) = \frac{\ln(S_t/K) + (r + 0.5\sigma^2)\tau}{\sigma\sqrt{\tau}}, \quad d_2(K) = d_1(K) - \sigma\sqrt{\tau}.$$

By the Breeden-Litzenberger formula, we can compute the risk neutral density of the underlying asset as follows:

$$q(x) \stackrel{\text{def}}{=} e^{r\tau} \frac{\partial^2 C_t(K, \tau)}{\partial K^2} \Big|_{K=x},$$

where $q(x)$ is the risk neutral probability density of S_T , $C_t(K, \tau)$ is the time- t price of a European call option with strike K and maturity $\tau = T - t$.

Common practice to obtain the risk neutral density is to first apply some smoothing techniques to remove butterfly arbitrage in option prices, and then use the central difference method to approximate the second order derivative. However, as we will show later in the numerical experiment section, such methods will be highly sensitive to the number of market observations and will also have significant errors in reproducing the call option prices if the integral of the estimated density significantly deviates from 1.

Such numerical difficulties are not surprising considering that even small differences in prices can lead to significant variations in implied volatilities (IVs), particularly for near-maturity options. For the sake of numerical stability, instead of directly using the relationship between option prices and the risk neutral density, we express the risk neutral density as a function of the implied volatility and its derivatives, and compute the risk neutral density from IVs.

The risk neutral density as a function of implied volatility can be seen in [Benko et al., 2007]. Here φ is the pdf of a standard normal distribution, and $\sigma_t(K, \tau)$ is the time- t implied volatility of a European vanilla call option with strike K and time to maturity τ :

$$\begin{aligned} q(x) = & e^{r\tau} S_t \sqrt{\tau} \varphi(d_1(x)) \left[\frac{1}{x^2 \sigma_t(x, \tau) \tau} + \frac{2d_1(x)}{x \sigma_t(x, \tau) \sqrt{\tau}} \frac{\partial \sigma_t(K, \tau)}{\partial K} \Big|_{K=x} \right. \\ & + \frac{d_1(x) d_2(x)}{\sigma_t(x, \tau)} \left(\frac{\partial \sigma_t(K, \tau)}{\partial K} \Big|_{K=x} \right)^2 \\ & \left. + \frac{\partial^2 \sigma_t(K, \tau)}{\partial K^2} \Big|_{K=x} \right]. \end{aligned} \quad (5)$$

When this formulation is used practically, we also need to impose non-arbitrage conditions. Following the settings from [Brunner and Hafner, 2003], for a frictionless and arbitrage-free market, and for a given maturity T , we require the following:

- 1 Non-negativity: the risk neutral density is non-negative with $q(x) \geq 0, x \geq 0$.
- 2 Total probability condition: the risk neutral density integrates to one, $\int_0^\infty q(x) dx = 1$.
- 3 Martingale property: the risk neutral density correctly reprices all calls, $\int_0^\infty \max\{x - K, 0\} q(x) dx = e^{r\tau} C_t(K, \tau), K \geq 0$.

3.1 Adaptive Local Quadratic Estimation

Following [Benko et al., 2007], we take observed market IVs with noise and estimate the corresponding true IVs and its derivatives. It's assumed that an observed IV consists of a true IV and some noise: $\tilde{\sigma}_i = \sigma(K_i) + \varepsilon_i$, where $\tilde{\sigma}_i$ is the observed IV, $\sigma(K_i)$ is the unknown true IV to be estimated, K_i is the i th strike, and ε_i is some unknown noise. The local quadratic estimator $\hat{\sigma}(K)$ and its first and second order derivatives can be obtained by solving the following optimization problem,

$$\min_{\alpha_0, \alpha_1, \alpha_2} \sum_{i=1}^{n_\tau} \left\{ \tilde{\sigma}_i - \alpha_0 - \alpha_1 (K_i - K) - \alpha_2 (K_i - K)^2 \right\}^2 \mathcal{K}_h(K - K_i),$$

with

$$\hat{\sigma}(K) = \alpha_0, \quad \hat{\sigma}'(K) = \alpha_1, \quad \hat{\sigma}''(K) = 2\alpha_2.$$

Here, n_τ is the number of available options with time-to-maturity τ , $\mathcal{K}_h(K - K_i) \stackrel{\text{def}}{=} \frac{1}{h} \mathcal{K}\left(\frac{K - K_i}{h}\right)$ is a kernel function with bandwidth h . For example, the Epanechnikov kernel, $\mathcal{K}(u) = \frac{3}{4} (1 - u^2) I(|u| \leq 1)$, is used in [Benko et al., 2007]. Then the risk neutral density can be rewritten in terms of α_0 , α_1 and α_2 as below:

$$\hat{q}(K) = F\sqrt{\tau}\varphi(d_1) \left\{ \frac{1}{K^2\alpha_0\tau} + \frac{2d_1}{K\alpha_0\sqrt{\tau}}\alpha_1 + \frac{d_1d_2}{\alpha_0}(\alpha_1)^2 + 2\alpha_2 \right\},$$

where τ is again the time to maturity, $F = S_t e^{r\tau}$ is the forward price, and φ is the standard normal probability density function. To ensure non-negativity, we impose the following constraint on the above optimization problem:

$$F\sqrt{\tau}\varphi(d_1) \left\{ \frac{1}{K^2\alpha_0\tau} + \frac{2d_1}{K\alpha_0\sqrt{\tau}}\alpha_1 + \frac{d_1d_2}{\alpha_0}(\alpha_1)^2 + 2\alpha_2 \right\} \geq 0.$$

A constant bandwidth and a fixed kernel, the Epanechnikov kernel, were used in [Benko et al., 2007]. The latter could be extended, as in [Fengler and Hin, 2015], which uses a two-univariate spline kernel that can accommodate B-splines of any order. As for the former, a constant bandwidth, the choice for h could influence the accuracy of the estimation significantly. The original local quadratic regression model manually chooses a constant h for different market data and models. This is highly heuristic and can be unstable if we have little prior information about the market data.

Since \mathcal{K}_h is only nonnegative within the localization window $[K - h, K + h]$, points outside of this interval have no influence on the estimate $\hat{\sigma}(K)$. When h is too small, in regions with insufficient observations, not enough observations are in $[K - h, K + h]$. This leads to an estimation that is noisy and unstable. On the other hand, when h is too large, the quality of estimation deteriorates due to over-smoothing. In our implementations, instead of a constant h , we choose h adaptively so that the above window covers sufficient neighboring observations. Namely, we choose the number of points to be included in the localization window. Numerical results show that this approach leads to a more stable estimation, particularly when there are insufficient observations for extreme strikes. Adding more observations in such regions helps to achieve an estimation quality that is comparable to that in regions with abundant observations.

3.2 Lognormal Mixture Tail Approximation

In Section 3.1, we impose the non-negativity requirement **1**. Following [Brunner and Hafner, 2003], in this section, we impose the remaining two requirements **2** & **3** by modeling tails of the risk neutral density. We model the risk neutral density by a piecewise function:

$$q(x; \theta_L, \theta_U) = \begin{cases} q^L(x; \theta_L), & x < K_L, \\ q^M(x), & K_L \leq x \leq K_U, \\ q^U(x; \theta_U), & x > K_U. \end{cases}$$

Here L, U stand for the lower and upper bounds of observed strikes, θ_L, θ_U are the parameters corresponding to the left-tail and right-tail of the risk neutral density, respectively, and $q^M(x)$ is the part of the density that is obtained in Section 3.1. It can be shown that the requirements **2** & **3** are equivalent to the following relations:

$$\int_0^{K_L} q^L(x; \theta_L) dx + \int_{K_U}^\infty q^U(x; \theta_U) dx = 1 - \int_{K_L}^{K_U} q^M(x) dx, \quad (6)$$

$$-e^{r\tau} \frac{\partial C_t^M(K, \tau)}{\partial K} \Big|_{K=K_U} = \int_{K_U}^\infty q(x; \theta_L, \theta_U) dx, \quad (7)$$

$$1 + e^{r\tau} \frac{\partial C_t^M(K, \tau)}{\partial K} \Big|_{K=K_L} = 1 - \int_{K_L}^\infty q(x; \theta_L, \theta_U) dx, \quad (8)$$

$$F_t(\tau) = \int_0^{K_L} x q^L(x; \theta_L) dx + \int_{K_L}^{K_U} x q^M(x) dx + \int_{K_U}^\infty x q^U(x; \theta_U) dx, \quad (9)$$

where $F_t(\tau)$ is the forward price.

We model each tail of the risk neutral density by a mixture of two log-normal distributions, namely:

$$q^i(x; \theta_i) = \lambda_i \ell(x; \eta_{i,1}, v_{i,1}^2) + (1 - \lambda_i) \ell(x; \eta_{i,2}, v_{i,2}^2), \quad \lambda_i \in [0, 1], i \in \{L, U\},$$

where the lognormal density function is defined as:

$$\ell(x; \eta_{i,j}, v_{i,j}^2) = \frac{1}{x v_{i,j} \sqrt{2\pi}} \exp\left(-\frac{1}{2} \left(\frac{\ln(x) - \ln(\eta_{i,j}) + \frac{v_{i,j}^2}{2}}{v_{i,j}}\right)^2\right), \quad j = 1, 2; i \in \{L, U\},$$

and $\theta_i = (\lambda_i, \eta_{i,1}, v_{i,1}^2, \eta_{i,2}, v_{i,2}^2)'$ for $i \in \{L, U\}$. The reason to model each tail by a mixture of two lognormal distributions is that a single lognormal distribution is not flexible enough for us to solve the system 6 to 9 and meet the non-arbitrage requirements. Note that $\eta_{i,j}$ is the expected value of the corresponding lognormal distribution. If we define $\mu_{i,j} = \ln(\eta_{i,j}) - \frac{1}{2}v_{i,j}^2$, then $\mu_{i,j}$ is the expected value of the corresponding normal distribution, which is more familiar.

We further impose the following boundary conditions for smoothness of the risk neutral density:

$$\left. \frac{\partial q^L(x; \theta_L)}{\partial x} \right|_{x=K_L} = \left. \frac{\partial q^M(x)}{\partial x} \right|_{x=K_L} \quad \text{and} \quad \left. \frac{\partial q^U(x; \theta_U)}{\partial x} \right|_{x=K_U} = \left. \frac{\partial q^M(x)}{\partial x} \right|_{x=K_U},$$

The ten-parameter nonlinear system can be reduced to a nonlinear equation with one parameter, which can be solved numerically by standard one-dimensional root-finding methods. Details can be seen in [Brunner and Hafner, 2003]. The relationships between the parameters are:

$$N(z_i) = N(d_2(K_i)) - K_i n(d_2(K_i)) \sqrt{\tau} \frac{\partial \sigma_t(K, \tau)}{\partial K} \Big|_{K=K_i}, \quad i \in \{L, U\}, \quad (10)$$

$$\lambda_i = \frac{q^M(K_i) - \frac{1}{K_i v_{i,2} \sqrt{2\pi}} e^{-\frac{1}{2}z_i^2}}{\frac{1}{K_i v_{i,1} \sqrt{2\pi}} e^{-\frac{1}{2}z_i^2} - \frac{1}{K_i v_{i,2} \sqrt{2\pi}} e^{-\frac{1}{2}z_i^2}}, \quad (11)$$

$$\eta_{i,1} = K_i e^{z_i v_{i,1} + \frac{v_{i,1}^2}{2}}, \quad \eta_{i,2} = K_i e^{z_i v_{i,2} + \frac{v_{i,2}^2}{2}}, \quad (12)$$

$$v_{i,1} = \frac{q^M(K_i) - \frac{1}{K_i v_{i,2} \sqrt{2\pi}} e^{-\frac{1}{2}z_i^2}}{\left(q^M(K_i) + K_i \frac{\partial q^M}{\partial x} \Big|_{x=K_i}\right) \frac{1}{z_i} - \frac{q^M(K_i)}{v_{i,2}}}, \quad (13)$$

$$\begin{aligned} & \lambda_L \eta_{L,1} N(-z_L - v_{L,1}) + (1 - \lambda_L) \eta_{L,2} N(-z_L - v_{L,2}) \\ &= F_t(\tau) N(-d_1(K_L)) + K_L^2 n(d_2(K_L)) \sqrt{\tau} \frac{\partial \sigma_t(K, \tau)}{\partial K} \Big|_{K=K_L}, \end{aligned} \quad (14)$$

$$\begin{aligned} & \lambda_U \eta_{U,1} N(z_U + v_{U,1}) + (1 - \lambda_U) \eta_{U,2} N(z_U + v_{U,2}) \\ &= F_t(\tau) N(d_1(K_U)) - K_U^2 n(d_2(K_U)) \sqrt{\tau} \frac{\partial \sigma_t(K, \tau)}{\partial K} \Big|_{K=K_U}. \end{aligned} \quad (15)$$

Here $n(\cdot)$ is the standard normal pdf and $N(\cdot)$ is the standard normal cdf.

Finally, to prevent calendar arbitrage, we require that the risk neutral densities for different maturities satisfy

$$\int_0^\infty \max\{x - K, 0\} \left(e^{r(T_{i+1}-T_i)} q_{S_{T_{i+1}}}(x) - q_{S_{T_i}}(x e^{-r(T_{i+1}-T_i)}) \right) dx \geq 0, \quad (16)$$

for all maturities $T_i \leq T_{i+1}$.

4 Optimality and Convergence of Numerical Convolution

In this section, we demonstrate optimal numerical parameter selection and convergence of the trapezoidal rule for numerical convolution in Bass-LV implementation. In particular, we assume limited smoothness in the marginal distribution functions and their inverses, as commonly encountered in numerical implementations involving spline interpolation and extrapolation.

Before analyzing numerical convergence, let us recall the following operator in the Bass-LV model:

$$\mathcal{A}F := F_{\mu_i} \circ \left(K_{T_{i+1}-T_i} \star \left(F_{\mu_{i+1}}^{-1} \circ \left(K_{T_{i+1}-T_i} \star F \right) \right) \right).$$

Here, K represents the heat kernel, \star denotes convolution, and \circ is function composition. The analysis of this operator's properties relies on results from [Conze and Henry-Labordere, 2021], which we now summarize:

Lemma 2.2 in [Conze and Henry-Labordere, 2021] establishes that $\mathcal{A}(\mathcal{E}) \subset \mathcal{E}$, where \mathcal{E} is the space of cumulative distribution functions. This ensures that each iteration produces a well-defined CDF.

Furthermore, Theorem 2.4 in [Conze and Henry-Labordere, 2021] demonstrates that $\mathcal{A}(\mathcal{E})$ is uniformly bounded and Lipschitz. By the Arzelà-Ascoli theorem, this implies that \mathcal{A} is continuous in the sup-norm and $\mathcal{A}(\mathcal{E})$ is relatively compact. Since \mathcal{E} is convex and closed, Schauder's fixed point theorem guarantees the existence of a solution in \mathcal{E} for the fixed point problem $F = \mathcal{A}F$. This solution is the $F_{W_{T_i}}$ that we are seeking in the Bass-LV implementation.

Given two consecutive maturities T_i, T_{i+1} , the following multi-layer integration needs to be done in solving the fixed-point problem:

$$\begin{aligned} & F_{\mu_i} \left(\left(K_{T_{i+1}-T_i} \star F_{\mu_{i+1}}^{-1} \left(K_{T_{i+1}-T_i} \star F \right) \right) (w) \right) \\ &= F_{\mu_i} \left(\int_{-\infty}^{\infty} \rho(y) \cdot (F_{\mu_{i+1}}^{-1} (K_{T_{i+1}-T_i} \star F))(w-y) dy \right) \\ &= F_{\mu_i} \left(\int_{-\infty}^{\infty} \rho(y) \cdot F_{\mu_{i+1}}^{-1} \left(\int_{-\infty}^{\infty} F(w-y-x)\rho(x) dx \right) dy \right). \end{aligned} \quad (17)$$

where $\rho(\cdot)$ is given by the heat kernel $K_{T_{i+1}-T_i}$, and $F(w)$ is the distribution obtained in a previous iteration that, upon convergence of the algorithm, yields the final distribution $F_{W_{T_i}}$.

In practice, the marginal distributions F_{μ_i} , its inverse $F_{\mu_i}^{-1}$, and the intermediate iterate F are never given in closed form. Instead, they are computed on a finite grid and interpolated (and, where necessary, extrapolated) with cubic or other splines. Our theoretical analysis is established based on such limited smoothness. To be specific, the smoothness order of a function refers to the highest order of continuous derivatives it possesses. A function with smoothness order m (denoted as C^m) has continuous derivatives up to order m .

Because splines are C^m for some finite m , the functions that actually enter (17) are automatically also C^m . In the analysis below, we make the following working assumption:

Assumption 1. $F_{\mu_i}, F_{\mu_i}^{-1}, F$ are piecewise polynomial and belong to C^m for some fixed and finite m .

Note that this assumption ensures smoothness at the knots between different polynomial segments while guaranteeing that the functions as a whole are in C^m . With this assumption, we have the following proposition:

Proposition 1. Given assumption 1, both the internal and external integrands in Eq.17 are well-defined in the following weighted Sobolev space

$$\mathcal{H}_m := \left\{ f \in L_\rho^2 \mid \|f\|_m := \left(\sum_{\tau=0}^m \|f^{(\tau)}\|_{L_\rho^2}^2 \right)^{1/2} < \infty \right\},$$

where $\rho(x) = \frac{1}{\sqrt{2\pi\sigma^2}} e^{-\frac{x^2}{2\sigma^2}}$, $\sigma^2 = T_{i+1} - T_i$, $L_\rho^2 := L_\rho^2(\mathbb{R})$, $f^{(\tau)} \in L_\rho^2$ for $\tau = 1, \dots, m$. The convergence rate of Gauss-Hermite quadrature for the above integrals can achieve $\mathcal{O}(n^{-m/2})$, where n stands for the number of quadrature points, m stands for the order of smoothness for the integrands.

In the following, we present results for the optimal step size and truncation level when the trapezoidal rule is used for the above numerical convolution, and give the corresponding convergence rate. We first give the trapezoidal scheme for the integral in Eq.17 as follows:

$$\sum_{m=-M}^M \rho(mh) \cdot F_{\mu_{i+1}}^{-1} \left(\sum_{n=-N}^N F(w-mh-nh)\rho(nh)h \right) \cdot h, \quad (18)$$

where h is step size, M and N represent the number of terms used in the trapezoidal scheme, and Mh and Nh are the level of truncation when integrals on the whole real line are replaced by integrals on finite intervals.

Following the idea of proposition 4.2 in [Kazashi et al., 2023], we can derive the following optimal setting for the step size and truncation level for trapezoidal rule based numerical convolution in Eq.17:

Proposition 2. *Given assumption 1. Let $\epsilon \in (\max\{1 - \sigma^2, 0\}, 1)$, where $\sigma^2 = T_{i+1} - T_i$. We have the following optimal parameter setting for the internal integral:*

$$Nh = \sqrt{\frac{2(T_{i+1} - T_i)}{(1 - \epsilon)} m \ln(2N + 1)},$$

$$h = \frac{\sqrt{\frac{2(T_{i+1} - T_i)}{(1 - \epsilon)} m \ln(2N + 1)}}{N}.$$

Optimal parameter setting for the external integral is similar. Under these optimal settings, the convergence rate of the trapezoidal rule for the above integrals can achieve $\mathcal{O}\left(\frac{(\ln n)^{(m/2+1/4)}}{n^m}\right)$, where n stands for the number of terms used in the trapezoidal schemes, and m stands for the order of smoothness for the integrands.

We conclude that, for any given convolution integral, when the same number of points are used, the convergence rate of the trapezoidal rule is $\mathcal{O}\left(\frac{(\ln n)^{(m/2+1/4)}}{n^m}\right)$ which is faster than the Gauss Hermite quadrature with a rate of $\mathcal{O}(n^{-m/2})$. This provides a theoretical foundation for using the trapezoidal rule for the numerical convolutions in the implementation of the Bass-LV model.

5 Numerical Experiments

5.1 Step-by-Step Calibration Procedure

In this section, we outline a step-by-step procedure for calibrating the Bass-LV model from European vanilla options market data.

1. **Extract implied volatilities (IV) from market prices:** Begin with observed market prices of European vanilla options. Compute the implied volatilities for different strikes and maturities.
2. **Fit a local quadratic regression model:** Use the extracted IVs to fit a local quadratic regression (LQR) model. This involves solving the following optimization problem for α_0, α_1 , and α_2 :

$$\min_{\alpha_0, \alpha_1, \alpha_2} \sum_{i=1}^{n_\tau} \left\{ \tilde{\sigma}_i - \alpha_0 - \alpha_1 (K_i - K) - \alpha_2 (K_i - K)^2 \right\}^2 \mathcal{K}_h (K - K_i),$$

where \mathcal{K}_h is a kernel function with bandwidth h .

3. **Calculate the risk neutral density:** Using α_0, α_1 , and α_2 obtained above, compute the risk neutral density $q^{\mathcal{M}}(x)$ on the interval $\mathcal{M} = [K_L, K_U]$ as follows:

$$q^{\mathcal{M}}(x) = F\sqrt{\tau}\varphi(d_1) \left\{ \frac{1}{x^2\alpha_0\tau} + \frac{2d_1}{x\alpha_0\sqrt{\tau}}\alpha_1 + \frac{d_1d_2}{\alpha_0}(\alpha_1)^2 + 2\alpha_2 \right\},$$

Here, K_L and K_U refer to the minimum and maximum observed strikes from the market data, respectively. After completing this step, one obtains the portion of the risk neutral density corresponding to the market observations.

4. **Construct the tails of the risk neutral density:** Use mixture of lognormal distributions to construct tails of the risk neutral density. This can be achieved by leveraging the parameters obtained in the previous step and then solving the root-finding system in section 3.2. After completing this step, one obtains the risk neutral density on $[0, K_L]$ and $[K_U, \infty]$.
5. **Complete the risk neutral density:** Combine the densities from the steps above to form a complete risk neutral density $q(x; \theta_L, \theta_U)$:

$$q(x; \theta_L, \theta_U) = \begin{cases} q^L(x; \theta_L), & x < K_L \\ q^{\mathcal{M}}(x), & K_L \leq x \leq K_U \\ q^U(x; \theta_U), & x > K_U \end{cases}.$$

6. **Calibrate the Bass-LV model:** With the arbitrage-free risk neutral densities and the corresponding distributions obtained above as input, using trapezoidal numerical convolution, solve the fixed-point problem to perform the calibration. It involves iteratively calculating the following:

$$AF := F_{\mu_i} \circ \left(K_{T_{i+1}-T_i} \star \left(F_{\mu_{i+1}}^{-1} \circ \left(K_{T_{i+1}-T_i} \star F \right) \right) \right),$$

until convergence is achieved.

This step-by-step procedure provides a structured approach to calibrate the Bass-LV model.

5.2 Iteration and Calibration Errors

In the Bass construction, a fix-point problem needs to be solved iteratively. Following the practice in [Conze and Henry-Labordere, 2021], the stopping condition is specified by controlling the following iteration error measured in the infinite norm:

$$err_{itr} = \left\| F_{W_{T_i}}^{(p)} - F_{W_{T_i}}^{(p-1)} \right\|_{\infty}.$$

The iteration continues until the iteration error is less than a predetermined tolerance level. The iteration error tolerance naturally determines the quality of calibration. Let err_{cab} be the calibration error, which is the mean absolute percentage error of calibrated IVs:

$$err_{cab} = \frac{1}{L} \sum_{j=1}^L \left| \frac{IV_{cab}^j - IV_{True}}{IV_{True}} \right|.$$

Here L is the number of option strike prices considered. In the following experiments, we numerically investigate how calibration error depends on iteration error tolerance.

5.3 Experiments in the Black-Scholes-Merton Case

In this section, we examine the Bass-LV calibration in the Black-Scholes-Merton model. In this case, the marginal distributions and their inverse are known and hence do not introduce any implementation error. The exact solution of the fixed point problem is also available in closed-form. This allows us to examine how iteration error control in numerical solution of the fixed point problem impacts calibration performance. It also enables us to compare different integration schemes and highlight the advantages of trapezoidal numerical convolution.

Let μ_1, μ_2 and μ_3 be lognormal distributions, where the standard deviations of the corresponding normal distributions are $\sigma\sqrt{T_1}, \sigma\sqrt{T_2}$ and $\sigma\sqrt{T_3}$, respectively. In this case, the solution to the fixed point problem is $F_{W_{T_i}} = \mathcal{N}\left(\frac{\cdot}{\sqrt{T_i}}\right)$ and $f(t, w) = S_0 \exp\left(-\frac{1}{2}\sigma^2 t + \sigma w\right)$.

In our experiment, the current time is $T_0 = 0$. Options with the following maturities are considered: $T_1 = 1, T_2 = 1.2$ and $T_3 = 1.5$. The initial asset price is $S_0 = 100$, the true IV is $\sigma = 1$, and the risk-free interest rate is $r = 0$. The details of the experiment are given in Algorithm 1 below.

Algorithm 1 The Black-Scholes-Merton Case

- Step 1: Given the lognormal marginal distributions: $S_{T_1} \sim \mu_1, S_{T_2} \sim \mu_2, S_{T_3} \sim \mu_3$
- Step 2: Numerically solve the fixed-point problem to get $F_{W_{T_i}}$
- Step 3: Simulate the spot price process and estimate European call option prices
- Step 4: Compute the IVs associated with the above call prices and compare to the true IV

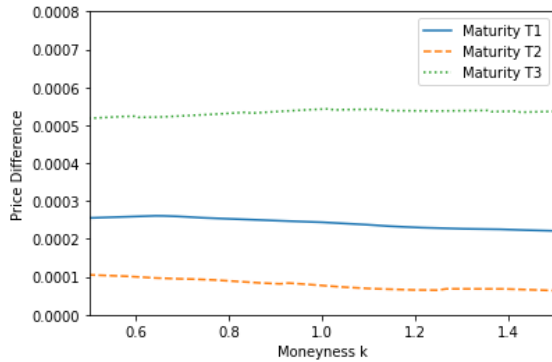


Figure 3: Pricing errors of options with maturities $T_1 = 1, T_2 = 1.2, T_3 = 1.5$ and moneyness $k = K/S_0$ in the calibrated Bass-LV model. Iteration error tolerance = 10^{-5} .

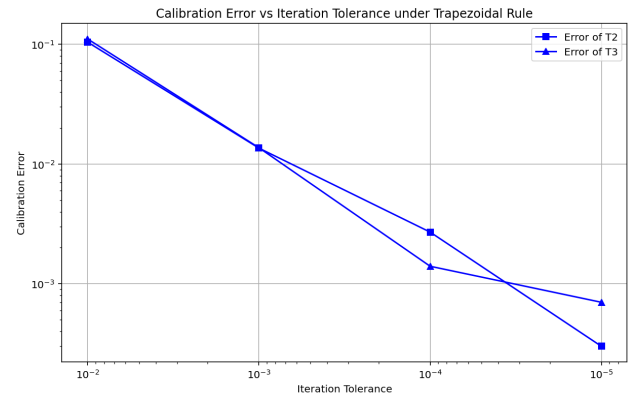


Figure 4: MAPE of calibrated implied volatility in the Black-Scholes-Merton case. Trapezoidal rule used for numerical integration.

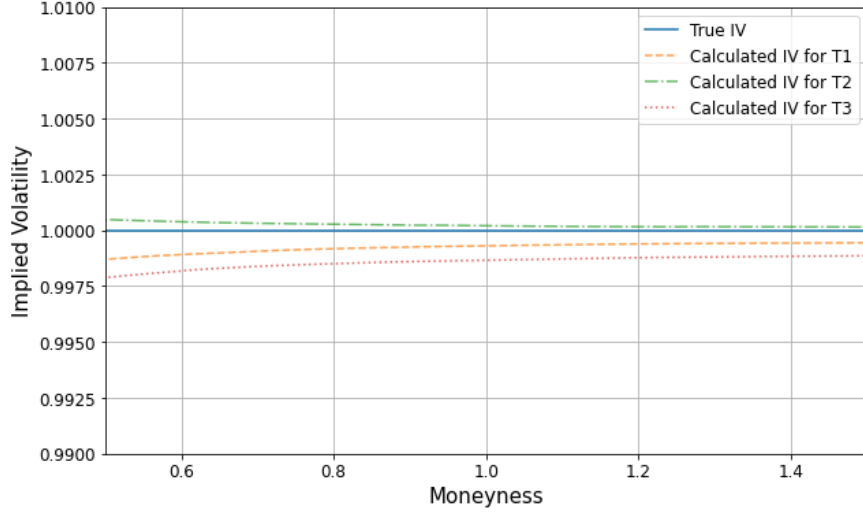


Figure 5: Calibrated IV in the Black-Scholes-Merton case for maturities $T_1 = 1$, $T_2 = 1.2$, $T_3 = 1.5$ and moneyness $k = K/S_0$.

Figure 3 shows that the absolute pricing errors of European call options with the above three maturities and various strikes are bounded by 6×10^{-4} in the calibrated model. Here, we consider option strike prices that are in $[0.5S_0, 1.5S_0]$. Options with these strikes are most actively traded. Figure 5 shows that the implied volatilities of the above options in the calibrated Bass-LV model are very close to the true IV, which is 1.

Iteration error tolerance in Figures 3 and 5 is set to 10^{-5} , i.e, the fixed point algorithm will stop when $\|F_{W_{T_i}}^{(p)} - F_{W_{T_i}}^{(p-1)}\|_{\infty} \leq 10^{-5}$ for some iteration index p .

In Figure 4, we show the numerical relationship between iteration error tolerance and calibration error. European option prices are computed using Monte Carlo simulation with sample size 3×10^8 . Calibrated IVs are then computed from these estimated option prices. When plotting err_{cab} , we re-run the Monte Carlo method several times with different random seeds and plot the median err_{cab} . This is to mitigate the impact of noisy random number generators and show a clearer relationship between iteration error tolerance and calibration accuracy. Since no fixed point problem needs to be solved for options with maturity T_1 , we didn't plot the error for this maturity.

As can be seen in Figure 4, as the iteration error tolerance decreases, calibration accuracy improves approximately linearly. In this particular example, to get a calibration error of 1%, an iteration error tolerance of about 10^{-3} is needed. In numerical experiments in [Conze and Henry-Labordere, 2021], an iteration error tolerance of 2×10^{-3} was used. However, when higher accuracy levels are desired in some applications, one must use a much smaller iteration error tolerance. For example, if the desired calibration error is 0.01%, an iteration error tolerance of 10^{-5} would be needed. In such cases, trapezoidal rule based numerical integration schemes clearly become more advantageous compared to the Gauss-Hermite quadrature, as to be shown next. Note that the calibration error for maturity T_3 flattens after reaching 10^{-3} . This is due to not large enough Monte Carlo sample size. Consequently, error due to Monte Carlo estimation starts to dominate. Increasing Monte Carlo sample size or using variance reduction techniques will help further reducing the calibration error.

Figure 6 compares the performance of Gauss-Hermite quadrature and the trapezoidal rule under different iteration error tolerance settings. The horizontal axis is the minimal amount of time the numerical solution of the fixed point problem takes to achieve the smallest possible calibration accuracy. It shows that, as the iteration error tolerance decreases, the computational time required when using the trapezoidal rule becomes much smaller compared to Gauss Hermite quadrature. This clearly shows the advantage of using the trapezoidal rule, in particular, when the desired accuracy level is high.

Our numerical results also support the linear convergence theory of the Bass calibration process presented in [Acciaio et al., 2023]. Figure 7 clearly shows that, for a given maturity, the number of iterations needed to solve the fixed point problem grows linearly in the logarithm of the iteration error tolerance. In later numerical experiments, we show that this is also roughly true in much more general settings than those specified in [Acciaio et al., 2023].

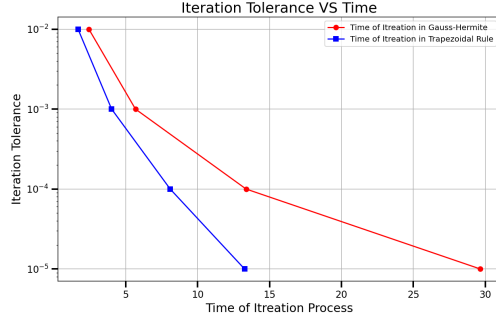


Figure 6: Time for solving fixed point problems in the Black-Scholes-Merton model: trapezoidal rule vs. Gauss-Hermite quadrature

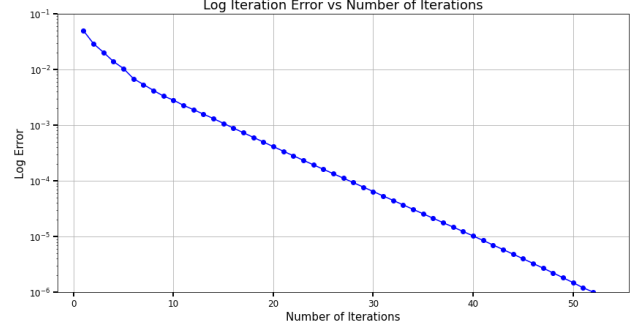


Figure 7: Iteration error tolerance vs. number of iterations needed to solve the fixed point problem in the Black-Scholes-Merton model

Tables 1 and 2 provide detailed results for the plots. These experiments were conducted using a 14th Gen Intel(R) Core(TM) i9-14900HX CPU @ 2.20 GHz and Python 3.11.9. All subsequent experiments are performed within this environment. The first column contains the iteration error tolerance. The second column contains the minimal amount of time needed to solve the fixed point problem to achieve the smallest possible calibration error. For the third column, note that no fixed point problem is solved for the first maturity. The error here is totally due to Monte Carlo estimation, hence identical for different iteration error tolerance levels. The last two columns contain the calibration errors for the remaining two maturities.

Table 1: Time and calibration error in the Black-Scholes-Merton model: Gauss Hermite quadrature

Iteration tolerance	Iteration time (seconds)	Calibration error (T_1)	Calibration error (T_2)	Calibration error (T_3)
1.0e-2	2.4	8.0e-4	1.1e-1	1.1e-1
1.0e-3	5.7	8.0e-4	1.3e-2	1.4e-2
1.0e-4	13.4	8.0e-4	2.3e-3	2.1e-3
1.0e-5	29.7	8.0e-4	3.0e-4	6.0e-4

Table 2: Time and calibration error in the Black-Scholes-Merton model: trapezoidal rule

Iteration tolerance	Iteration time (seconds)	Calibration error (T_1)	Calibration error (T_2)	Calibration error (T_3)
1.0e-2	1.7	8.0e-4	1.0e-1	1.1e-1
1.0e-3	4.0	8.0e-4	1.4e-2	1.4e-2
1.0e-4	8.1	8.0e-4	2.7e-3	1.4e-3
1.0e-5	13.3	8.0e-4	3.0e-4	7.0e-4

5.4 Comparison with the Breeden-Litzenberger Approach

Generating the risk neutral density is one of the most important steps in Bass LV calibration. In this section, we compare our proposed method with the widely used Breeden-Litzenberger formula. The Breeden-Litzenberger approach usually starts with cleaning and smoothing the market prices to meet non-arbitrage conditions. The risk neutral density is then derived using the formula:

$$q(x) \stackrel{\text{def}}{=} e^{r\tau} \frac{\partial^2 C_t(K, \tau)}{\partial K^2} \Big|_{K=x}.$$

To eliminate the need for the non-trivial price cleaning and smoothing step for the Breeden-Litzenberger approach, we generate arbitrage-free option prices and use them as "market" data. The experiment is done in the Stochastic Volatility Inspired (SSVI) model from [Gatheral and Jacquier, 2014].

Given the arbitrage-free option price surface generated in this model, we apply the Breeden-Litzenberger formula to derive the risk neutral densities for different maturities using finite difference.

Our proposed method on the other hand is rather robust, even when market data contains noise. To numerically illustrate this, we add some random noise to the arbitrage-free SSVI surface. This produces a pseudo-market IV surface with potential arbitrage. We then apply our proposed method to generate risk neutral densities and corresponding marginal distributions for different maturities. An outline of the experiments in the SSVI case is in Algorithm 2.

Algorithm 2 The SSVI Case

Step 1: Generate "market" data from the SSVI model. Add random noise. Apply the LQR method to construct the central part of the risk neutral density.

Step 2: Use lognormal mixture to construct the tails of the risk neutral density.

Step 3: Numerically solve the fixed-point problem to get $F_{W_{T_i}}$

Step 4: Simulate the spot price process and estimate European call option prices

Step 5: Compute the IVs associated with the above call prices and compare to the true IVs.

Recall that for the Heston-like SSVI model presented in [Gatheral and Jacquier, 2014], the function φ is defined as:

$$\varphi(\theta_t) = \frac{1}{\lambda\theta_t} \left\{ 1 - \frac{1 - e^{-\lambda\theta_t}}{\lambda\theta_t} \right\},$$

where $\lambda \geq \frac{(1+|\rho|)}{4}$ ensures no arbitrage. The total variance surface is given by:

$$w(k, \theta_t) = \frac{\theta_t}{2} \left\{ 1 + \rho\varphi(\theta_t)k + \sqrt{(\varphi(\theta_t)k + \rho)^2 + (1 - \rho^2)} \right\}.$$

The corresponding IV surface is then obtained via

$$\sigma(k, t) = \sqrt{\frac{w(k, \theta_t)}{t}}, \quad (19)$$

where k represents log moneyness, i.e.

$$e^k = \frac{K}{S_0 e^{r\tau}},$$

with τ being the time to maturity and K the strike price.

In this model, the risk neutral density can be computed analytically. This allows us to examine the quality of the risk neutral densities estimated using both the proposed method and the Breeden-Litzenberger approach. More specifically, by computing σ , σ' , σ'' and using equation 5, we can obtain the closed-form expression for the true risk neutral density to serve as a benchmark.

For our experiment, we set the parameters as follows: $\rho = 0.3$, $\lambda = \frac{(1+|\rho|)}{4} + 1$, and $\theta_t = 0.4t$. The initial spot price is set at $S_0 = 100$. The risk-free rate is $r = 0$. Figure 8 illustrates the resulting SSVI surface.

Suppose the first option maturity to be considered is $T_1 = 2$. Given the previously generated IVs with random noise, Figure 9 presents the recovered IVs using local quadratic regression (LQR). Despite the presence of noise and potential arbitrage in the inputs, the LQR method effectively recovers the true IV with great accuracy. From IVs calibrated using local quadratic regression, we construct the lognormal mixture tails. Table 3 shows the parameters obtained, where K_L and K_U represents the minimal and maximal observed strike prices. Figure 10 shows the corresponding estimated risk neutral density with lognormal mixture tails.

Table 3: Parameters for Lognormal Mixture Tails

Parameter	Lower (i=L)	Upper (i=U)
λ_i	0.879196378130754	0.021345797160246
$v_{i,1}$	0.999932326888895	0.138484172035767
$v_{i,2}$	0.696842788545524	0.946507489626882
$\mu_{i,1}$	-0.035711890633837	0.326246597279264
$\mu_{i,2}$	-0.876812461936515	-0.507637416676997
K_i	6.016806722689075	159.8655462184874

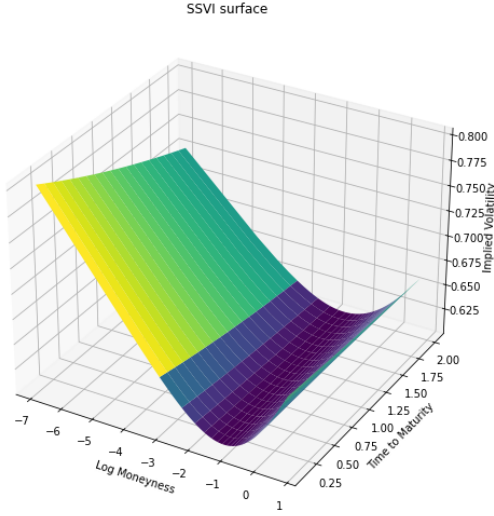


Figure 8: Heston-like SSVI implied volatility surface

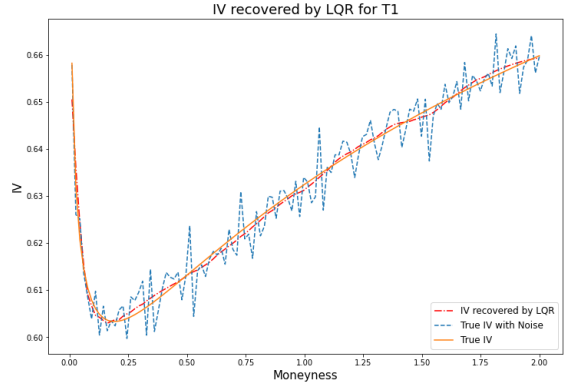


Figure 9: IVs recovered by local quadratic regression for maturity T_1 from data with noise

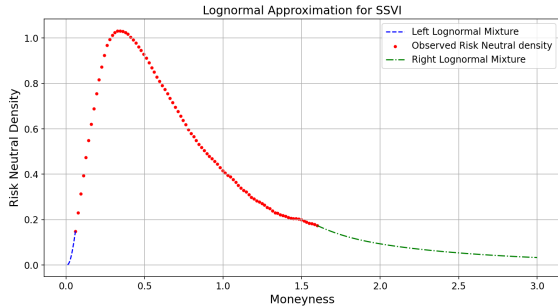


Figure 10: Estimated risk neutral density with lognormal-mixture tails from data with noise

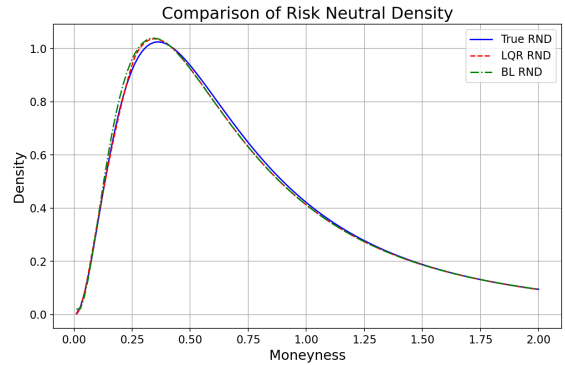


Figure 11: Estimated risk neutral density: proposed method vs Breeden-Litzenberger

To compare to the Breeden-Litzenberger approach, we consider a range of $[6, 160]$ for the strike price. For the Breeden-Litzenberger approach, spline interpolation and extrapolation are used, with boundary conditions ensuring well-defined extrapolations. To optimize the performance of the Breeden-Litzenberger method, we use 120 evenly spaced strike prices ranging from 5 to 200, since the performance of the Breeden-Litzenberger method relies heavily on the accuracy of finite difference, which requires a larger number of observations.

Under these settings, we compare the two approaches in Figures 11, 12, and 13. In Figure 11, "LQR RND" shows the risk neutral density constructed using our proposed approach with local quadratic regression and lognormal mixture tails. "BL RND" represents the risk neutral density constructed using the Breeden-Litzenberger method. "True RND" represents the true risk neutral density in the Heston-like SSVI model.

Although both "LQR RND" and "BL RND" seem to be close to the true risk neutral density, our proposed method provides a more accurate estimation. Figure 12 shows the absolute error for both estimated risk neutral densities. It can be seen that the proposed method (dashed line) achieves better accuracy compared to the Breeden-Litzenberger method (solid line). The latter shows notable errors for moneyness that is low. This leads to much larger errors for calibrated implied volatilities. In Figure 13, we compare the implied volatilities (IVs) obtained from both methods to true IVs (represented by the dashed line). The solid curve, generated using the Breeden-Litzenberger method, deviates significantly from the true IV. In contrast, IVs calculated using our proposed method (represented by the dash-dotted line) closely align with the true IV.

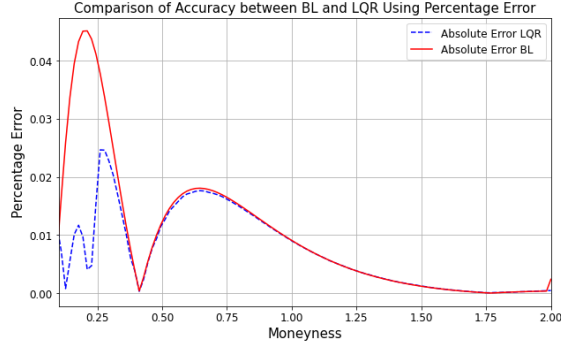


Figure 12: Estimation error for risk neutral density: proposed method vs Breeden-Litzenberger

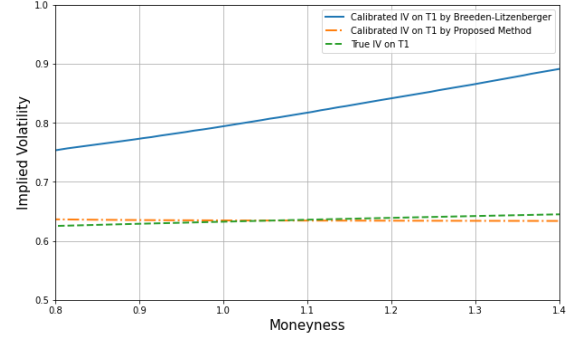


Figure 13: Calibrated IV: proposed method vs Breeden-Litzenberger

5.5 Numerical Experiment Based on TSLA Market Data

We conduct an experiment using the TSLA market data on July 1st, 2020. Since TSLA does not pay dividends, we treat the American call options as European call options and adjust the data to remove the effects of the interest rate term structure. The three maturities we select are 2020/09/18, 2020/10/16, and 2021/01/15, when sufficient market observations were available for call options. The option data was sourced from OptionMetrics.

Since the Bass construction assumes a zero interest rate, the data need to be regularized accordingly. Assuming the starting maturity is $T_0 = 0$, the forward price at time t is given by $F(t) = S_0 e^{rt}$. We define the moneyness at time t as $km(t) = \frac{K(t)}{F(t)}$ where $K(t)$ is the real strike on time t . As such, the normalized call option price is calculated as:

$$C_N(t, km(t)) = \frac{C(t, K(t))}{F(t)}.$$

To avoid potential artificial jumps in implied volatility (IV) at the at-the-money (ATM) region, we applied a smoothing procedure to the IV curves. We use a blending approach as described in [Birru and Figlewski, 2010] and [Alexiou et al., 2023]. In this approach, the IVs of put and call options with strike prices within a specified range close to the underlying spot price S_0 are blended as follows:

$$\hat{IV}(K) = w \cdot IV_{put}(K) + (1 - w) \cdot IV_{call}(k),$$

with $w = \frac{K_{max} - K}{K_{max} - K_{min}}$, and K_{max} and K_{min} are the maximum and minimum strike prices of the range, respectively. For our experiment, we focus on calibrating the market smile on the call option side. We therefore choose the blending region as $(0.5S_0, S_0)$. For illustration, result of smoothing for maturity T1 is shown in Figure 14.

After cleaning and processing the data, we apply the LQR model to the three maturities to generate arbitrage-free IV curves and the corresponding values of the risk neutral densities. The fitted IV curve for maturity T1 is shown in Figure 15. The risk neutral density calculated based on this IV curve can be seen in Figure 16.

Then we complete the risk neutral densities with lognormal mixture tails, as described in Section 3.2. Note that the density in Figure 16 is bimodal, with a minor mode near zero. This could lead to numerical difficulties in solving the nonlinear system in Section 3.2. To address this, we slightly reduce the domain $[K_L, K_U]$ to exclude this region, and impose constraints $v_{L,1} \geq 1$, $v_{L,2} \in (0, 1)$, and $\lambda_L > 0.5$ to create a desired lognormal mixture tail on the left with a minor mode. Table 4 presents the parameters of the lognormal mixture tails for the risk neutral densities corresponding to all the three maturities. Figure 17 shows the risk neutral density completed with lognormal mixture tails for maturity T1. The thick black curve is computed from LQR fitted IVs, and the blue solid left tail and the red dashed right tail are lognormal mixtures with parameters given in the T1 column of Table 4.

After we obtain arbitrage-free risk neutral densities for all maturities, we use spline interpolation and extrapolation and compute the probability distribution functions and their inverse corresponding to the densities. These are required for the Bass construction.

Figure 18 depicts the relationship between calibration accuracy and iteration error tolerance for maturities T2 and T3. Detailed numerical results are provided in table 5 and 6. Option prices and the corresponding implied volatilities in the calibrated model are computed using Monte Carlo simulation with a sample size of around 7×10^6 . Note that no

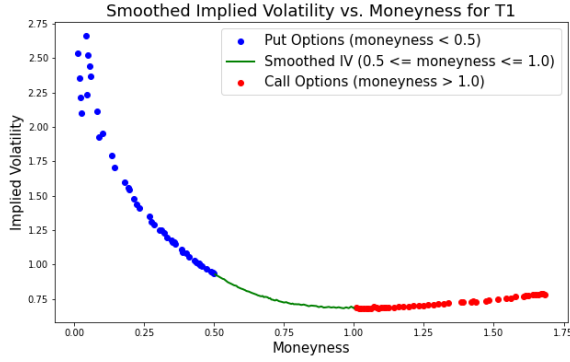


Figure 14: Smoothed IV for maturity T1

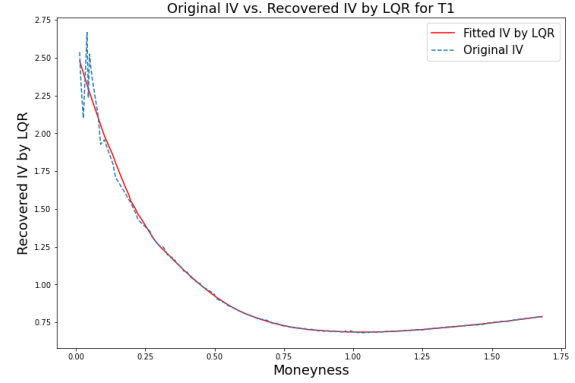


Figure 15: LQR fitted IV for T1

Table 4: Parameter settings for lognormal mixture tails

Parameters	T1	T2	T3
λ_L	0.891814729	0.730072506	0.999997865
v_{L1}	11.83540063	35.27086006	5.874220433
v_{L2}	0.389034015	0.442752001	0.117462989
μ_{L1}	25.61363809	75.02042380	9.323137361
μ_{L2}	-0.312016942	-0.153184102	-1.246629261
λ_U	0.818069793	0.927681918	0.971590088
v_{U1}	0.283361639	0.345919720	0.437880299
v_{U2}	1.167721500	1.708909349	2.078893403
μ_{U1}	-0.013315716	-0.065021265	-0.091679922
μ_{U2}	-1.408634421	-2.074760445	-1.947687673
L_{cdf}	0.011757319	0.015447680	0.033174055
U_{cdf}	0.957228077	0.929827574	0.870975267

fixed point problem needs to be solved for options pricing and calculating the IVs for the first maturity. By fixing the simulation random seeds, we obtain a constant calibration error, determined solely by the Monte Carlo sample size, for this maturity. Figure 18 and Tables 5, 6 show that reducing the iteration error tolerance from 10^{-2} to 10^{-3} significantly reduces the calibration error. However, reducing the tolerance further does not lead to further significant improvement, since the calibration error will eventually be dominated by the error due to Monte Carlo sample size.

Figure 19 compares the computational time needed for solving the fixed point problems using the trapezoidal rule and Gauss-Hermite quadrature. It shows that, when higher calibration accuracy is desired and hence smaller iteration error control level is used, the trapezoidal rule will be much faster and is hence preferred.

Figure 20 demonstrates the linear convergence of the fixed-point algorithm, as established in [Acciaio et al., 2023], in the TSLA case study. Finally, Figure 21 shows the implied volatilities of options prices calculated in the calibrated Bass-LV model. The iteration error tolerance is set at 10^{-4} . The Figure shows the effectiveness of the proposed methods in fitting even rather atypical market implied volatilities.

Table 5: Time and calibration error in the TSLA case: Gauss-Hermite quadrature

Iteration tolerance	Iteration time (seconds)	Calibration error (T_1)	Calibration error (T_2)	Calibration error (T_3)
1.0e-2	1.0	7.0e-3	4.8e-2	5.7e-2
1.0e-3	5.5	7.0e-3	1.7e-2	1.9e-2
1.0e-4	17.6	7.0e-3	8.5e-3	8.3e-3
1.0e-5	38.6	7.0e-3	8.4e-3	7.8e-3

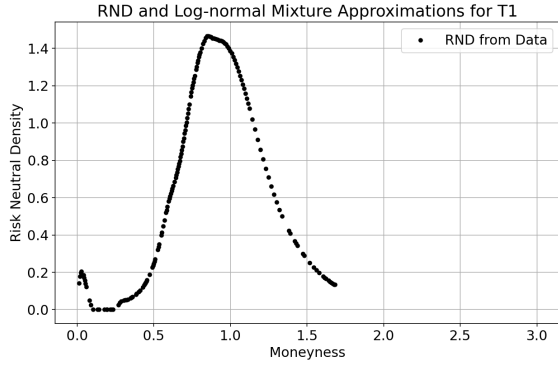


Figure 16: Risk neutral density for maturity T1 from LQR fitted implied volatility

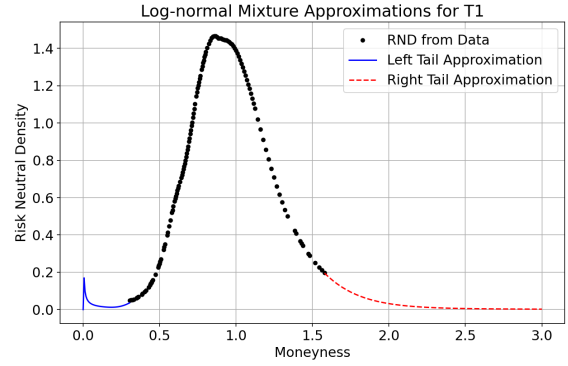


Figure 17: Lognormal mixture tails of the risk neutral density for maturity T1

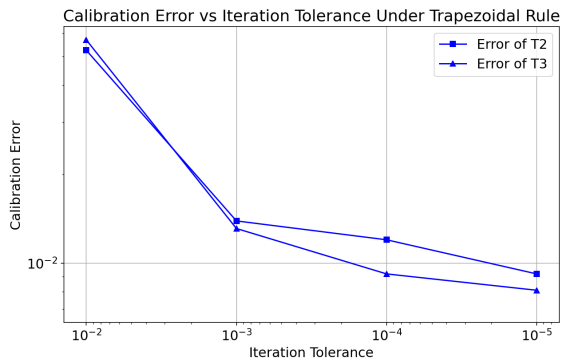


Figure 18: Calibration error vs. iteration error tolerance for the TSLA case

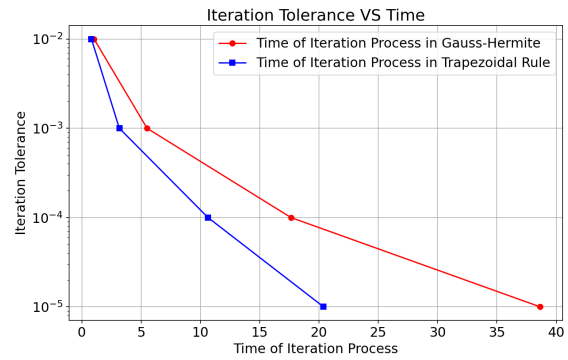


Figure 19: Time for solving fixed point problems in TSLA case: trapezoidal rule vs. Gauss Hermite quadrature

Table 6: Time and calibration error in the TSLA case: trapezoidal rule

Iteration tolerance	Iteration time (seconds)	Calibration error (T_1)	Calibration error (T_2)	Calibration error (T_3)
1.0e-2	0.8	7.0e-3	5.3e-2	5.0e-2
1.0e-3	3.2	7.0e-3	1.4e-2	1.3e-2
1.0e-4	10.6	7.0e-3	1.2e-2	9.2e-3
1.0e-5	20.4	7.0e-3	9.2e-3	8.1e-3

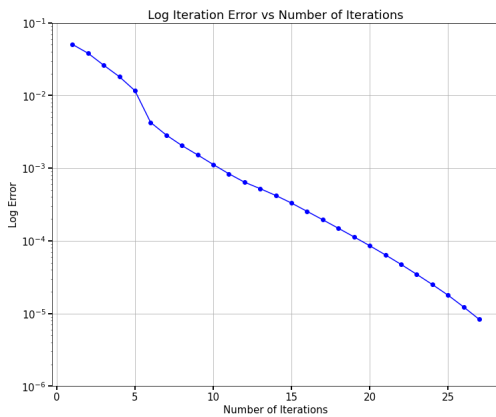


Figure 20: Log iteration error vs. number of iterations in TSLA case

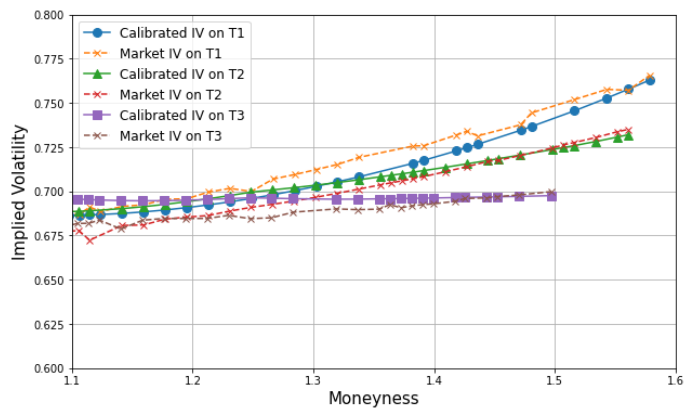


Figure 21: Observed IVs vs. IVs computed from option prices in the calibrated Bass-LV model: iteration error tolerance = 10^{-4}

6 Conclusions

This paper provides an easy to follow guidance for a practical and efficient implementation of the Bass-LV model. We propose a method that starts with computing arbitrage free implied volatilities from option price data using local quadratic regression. Risk neutral densities calculated from the implied volatilities are completed by lognormal mixture tails. This approach provides high quality marginal distributions that are necessary for a practical and efficient Bass LV calibration. Following the above, a series of fixed point problems need to be solved. Each iteration requires fast and accurate evaluation of two convolution integrals. We show theoretically and numerically that the simple trapezoidal rule is more accurate and faster than the commonly used Gauss-Hermite quadrature. Numerical experiments in standard options pricing models as well as in market case studies show that the proposed method for constructing risk neutral densities leads to great calibration robustness and accuracy, and the trapezoidal rule based numerical convolution outperforms Gauss-Hermite quadrature for faster calibration of Bass local volatility models.

7 Appendix - Proofs

7.1 Proof of proposition 1

Recall that for $m \in \mathbb{N}$, the weighted Sobolev space \mathcal{H}_m with the weight function $\rho(x) = \frac{1}{\sqrt{2\pi\sigma^2}} e^{-\frac{x^2}{2\sigma^2}}$ consists of functions $f \in L^2_\rho$ whose weak derivatives up to order m belong to L^2_ρ :

$$\mathcal{H}_m := \left\{ f \in L^2_\rho \mid \|f\|_m := \left(\sum_{\tau=0}^m \|f^{(\tau)}\|_{L^2_\rho}^2 \right)^{1/2} < \infty \right\},$$

where $L^2_\rho = \left\{ f : \mathbb{R} \rightarrow \mathbb{R} \mid \|f\|_{L^2_\rho}^2 = \int_{\mathbb{R}} |f(x)|^2 \rho(x) dx < \infty \right\}$.

By our construction, $F_{\mu_i}, F_{\mu_i}^{-1}, F \in C^m$ are piece-wise polynomial functions, and the convolution expression $\int_{\mathbb{R}} \rho(y) \cdot F_{\mu_{i+1}}^{-1} \left(\int_{\mathbb{R}} F(w - y - x) \rho(x) dx \right) dy$ shows that the inner and outer integrand shares the same structure: $\int f(x) \cdot \rho(x) dx$. To show the integrands belongs to \mathcal{H}_m , we only need to focus on the generic function $f \in C^m(\mathbb{R})$ with at most polynomial growth because of the spline method. That is, for each $k = 0, 1, \dots, m$, there exist constants $C_k, p_k > 0$ such that:

$$\left| f^{(k)}(x) \right| \leq C_k (1 + |x|^{p_k})$$

for all $x \in \mathbb{R}$.

For each $k = 0, 1, \dots, m$, we have:

$$\int_{\mathbb{R}} \left| f^{(k)}(x) \right|^2 \rho(x) dx \leq C_k^2 \int_{\mathbb{R}} (1 + |x|^{p_k})^2 \rho(x) dx$$

The integrand $(1 + |x|^{p_k})^2 \rho(x)$ behaves like $|x|^{2p_k} e^{-\frac{x^2}{2\sigma^2}}$ for large $|x|$. Since the Gaussian decay dominates any polynomial growth (that is, $\lim_{|x| \rightarrow \infty} |x|^p e^{-\frac{x^2}{2\sigma^2}} = 0$ for any power p), this integral is finite.

Therefore, $\int_{\mathbb{R}} \left| f^{(k)}(x) \right|^2 \rho(x) dx < \infty$ for all $k = 0, 1, \dots, m$, and with only finite terms of summations, it means $f \in \mathcal{H}_m$.

For the Gauss-Hermite quadrature applied to functions with this level of regularity, classical results in numerical analysis (Brass & Petras, 2011) establish that with n quadrature points, the approximation error is bounded by:

$$\left| \int_{\mathbb{R}} f(x) \rho(x) dx - \sum_{i=1}^n w_i f(x_i) \right| \leq C \cdot \|f^{(m)}\|_{L^2_\rho} \cdot n^{-m/2} \quad (20)$$

where C is a constant depending only on m , and $\|f^{(m)}\|_{L^2_\rho} = \left(\int_{\mathbb{R}} |f^{(m)}(x)|^2 \rho(x) dx \right)^{1/2}$.

Thus, the convergence rate of Gauss-Hermite quadrature for the numerical evaluation of the integrals in equation (17) is $\mathcal{O}(n^{-m/2})$, where m is the smoothness order of the functions involved.

Finally, by applying results from [Kazashi et al., 2023] and [Mastroianni and Monegato, 1994], we derive the convergence rate for Gauss-Hermite quadrature in the weighted Sobolev space \mathcal{H}_m . Specifically, for a function $f \in \mathcal{H}_m$, the Gauss-Hermite quadrature approximation $Q_n^{\text{GH}}(f)$ to the integral $I(f) := \int_{\mathbb{R}} f(x)\rho(x) dx$, where $\rho(x)$ is the Gaussian weight function, satisfies the following error bound:

$$|I(f) - Q_n^{\text{GH}}(f)| \leq Cn^{-m/2}\|f\|_m,$$

where n is the number of quadrature points, m is the smoothness order of the function f , $\|f\|_m$ is the norm in the weighted Sobolev space, and $C > 0$ is a constant independent of n .

This result shows that the convergence rate of the Gauss-Hermite quadrature depends on both the number of quadrature points n and the smoothness m of the function f . As n increases, the error decays at a rate proportional to $n^{-m/2}$, with smoother functions (i.e., higher m) leading to faster convergence. The constant C is determined by the specific properties of the function and the quadrature scheme but remains independent of the number of quadrature points.

To be brief, we conclude that in Bass-LV construction, the rate of convergence for Gauss-Hermite quadrature under finite smoothness condition can achieve $\mathcal{O}(n^{-m/2})$. Now we complete the proof for this part.

7.2 Proof of Proposition 2

Before deriving the optimality of the Trapezoidal Rule Scheme, we first present some properties of Hermite polynomials, which will be useful for our weighted function $\rho(x) = \frac{1}{\sqrt{2\pi\sigma^2}}e^{-\frac{x^2}{2\sigma^2}}$. Recall that the probabilist's Hermite polynomials are defined as:

$$H_{e_n}(x) = (-1)^n e^{\frac{x^2}{2}} \frac{d^n}{dx^n} e^{-\frac{x^2}{2}},$$

and satisfy the orthogonality relation:

$$\int_{-\infty}^{\infty} H_{e_m}(x)H_{e_n}(x)e^{-\frac{x^2}{2}} dx = \sqrt{2\pi n!}\delta_{nm},$$

where δ_{nm} is the Kronecker delta. We now state the following proposition:

Proposition 3. *The normalized Hermite polynomials with respect to $\rho(x)$ are given by:*

$$H_{e_n}^\sigma(x) = \frac{(-1)^n \sigma^n}{\sqrt{n!}} e^{\frac{x^2}{2\sigma^2}} \frac{d^n}{dx^n} e^{-\frac{x^2}{2\sigma^2}}, \quad x \in \mathbb{R},$$

and satisfy the recurrence relation:

$$(H_{e_n}^\sigma(x))' = \frac{\sqrt{n}}{\sigma} H_{e_{n-1}}^\sigma(x), \quad \forall n \geq 1.$$

Proof: First, we verify the normalization by calculating the L_ρ^2 norm:

$$\int_{-\infty}^{\infty} H_{e_n}^\sigma(x)H_{e_n}^\sigma(x)\rho(x)dx = 1.$$

This follows directly from applying the orthogonality relation of the Hermite polynomials, and adjusting for the scaling factor σ :

$$\begin{aligned} & \int_{-\infty}^{\infty} H_{e_n}^\sigma(x)H_{e_n}^\sigma(x)\frac{1}{\sqrt{2\pi\sigma^2}}e^{-\frac{x^2}{2\sigma^2}} dx \\ &= \frac{\sigma^{2n}}{n!\sqrt{2\pi}} \int_{-\infty}^{\infty} \left[e^{\frac{x^2}{2\sigma^2}} \frac{d^n}{dx^n} e^{-\frac{x^2}{2\sigma^2}} \right]^2 e^{-\frac{x^2}{2\sigma^2}} \frac{1}{\sigma} dx \\ &= \frac{\sigma^{2n}}{n!\sqrt{2\pi}} \int_{-\infty}^{\infty} \left[e^{\frac{y^2}{2}} \frac{1}{\sigma^n} \frac{d^n}{dy^n} e^{-\frac{y^2}{2}} \right]^2 e^{-\frac{y^2}{2}} dy \\ &= \frac{1}{n!\sqrt{2\pi}} \int_{-\infty}^{\infty} H_{e_n}(y)H_{e_n}(y)e^{-\frac{y^2}{2}} dy \\ &= \frac{1}{n!\sqrt{2\pi}} \sqrt{2\pi n!} = 1 \end{aligned}$$

The recurrence relation is derived using the chain rule on the differentiated form of $H_{e_n}^\sigma(x)$, applying the Leibniz rule for products of exponentials and polynomials:

$$\begin{aligned}
 (H_{e_n}^\sigma(x))' &= \frac{d}{dx} \left[\frac{(-1)^n \sigma^n}{\sqrt{n!}} e^{\frac{x^2}{2\sigma^2}} \frac{d^n}{dx^n} e^{-\frac{x^2}{2\sigma^2}} \right] \\
 &= \frac{(-1)^n \sigma^n}{\sqrt{n!}} \left[\frac{x}{\sigma^2} e^{\frac{x^2}{2\sigma^2}} \frac{d^n}{dx^n} e^{-\frac{x^2}{2\sigma^2}} + e^{\frac{x^2}{2\sigma^2}} \frac{d^{n+1}}{dx^{n+1}} e^{-\frac{x^2}{2\sigma^2}} \right] \\
 &= \frac{(-1)^n \sigma^n}{\sqrt{n!}} \left[\frac{x}{\sigma^2} e^{\frac{x^2}{2\sigma^2}} \frac{d^n}{dx^n} e^{-\frac{x^2}{2\sigma^2}} + e^{\frac{x^2}{2\sigma^2}} \left(-\frac{x}{\sigma^2} \frac{d^n}{dx^n} e^{-\frac{x^2}{2\sigma^2}} - \frac{n}{\sigma^2} \frac{d^{n-1}}{dx^{n-1}} e^{-\frac{x^2}{2\sigma^2}} \right) \right] \\
 &= \frac{(-1)^n \sigma^n}{\sqrt{n!}} \left[-\frac{n}{\sigma^2} e^{\frac{x^2}{2\sigma^2}} \frac{d^{n-1}}{dx^{n-1}} e^{-\frac{x^2}{2\sigma^2}} \right] \\
 &= \frac{(-1)^{n+1} n \sigma^{n-2}}{\sqrt{n!}} e^{\frac{x^2}{2\sigma^2}} \frac{d^{n-1}}{dx^{n-1}} e^{-\frac{x^2}{2\sigma^2}} \\
 &= \frac{(-1)^{n+1} n \sigma^{n-2} \sqrt{(n-1)!}}{\sqrt{n} \cdot \sqrt{(n-1)!}} H_{e_{n-1}}^\sigma(x) \\
 &= \frac{\sqrt{n}}{\sigma} H_{e_{n-1}}^\sigma(x)
 \end{aligned}$$

We will use this result to bound the norms of the function in the next part of the proof.

Lemma 1 (Bounded Norms). Assume the inner integrand of the Bass-LV construction has m -order smoothness. Let $F_i(x) := F(w - x - y) \cdot \rho(x)$, where F is the distribution obtained in a previous iteration, w, y are constants, and $\rho(x) = \frac{1}{\sqrt{2\pi\sigma^2}} e^{-\frac{x^2}{2\sigma^2}}$ is the Gaussian weight function. For the τ -th order derivative of $F_i(x)$, we have the following bounds:

$$\|F_i^{(\tau)}(x)\|_{L^1(\mathbb{R})} < \infty, \quad \|F_i^{(m)}(x)\|_{L^2(\mathbb{R})} < \infty, \quad \sup_{x \in \mathbb{R}} \left| e^{(1-\varepsilon)\frac{x^2}{2\sigma^2}} F_i^{(\tau)}(x) \right| < \infty,$$

where ε is a small positive constant such that $\frac{1-\varepsilon}{\sigma^2} \in (0, 1)$.

Proof: Since our weighted function is heat kernel with zero drift, it aligns with the form of Hermite quadrature we constructed in proposition 3. We can write under chain rule that:

$$\begin{aligned}
 \|F_i^{(\tau)}\|_{L^1(\mathbb{R})} &\leq \sum_{k=0}^{\tau} \binom{\tau}{k} \|F^{(\tau-k)}(w - x - y) \cdot \rho^{(k)}(x)\|_{L^1} \\
 &= \sum_{k=0}^{\tau} \binom{\tau}{k} \left(\int_{\mathbb{R}} |F^{(\tau-k)}(w - x - y) \frac{(-1)^k}{\sigma^k} \sqrt{k!} H_{e_k}^\sigma(x) \frac{1}{\sqrt{2\pi\sigma^2}} e^{-\frac{x^2}{2\sigma^2}} | dx \right) \\
 &\text{(Applying Hölder's Inequality)} \\
 &\leq \sum_{k=0}^{\tau} \binom{\tau}{k} \frac{\sqrt{k!}}{\sigma^k} \left(\int_{\mathbb{R}} |F^{(\tau-k)}(w - x - y)|^2 \rho(x) dx \right)^{1/2} \left(\int_{\mathbb{R}} |H_{e_k}^\sigma(x)|^2 \rho(x) dx \right)^{1/2}.
 \end{aligned}$$

Given the analysis in proposition 1, we know that $F \in C^m(\mathbb{R})$ with at most polynomial growth. This means that $\left(\int_{\mathbb{R}} |F^{(\tau-k)}(w - x - y)|^2 \rho(x) dx \right)$ is bounded by some constant:

$$\left(\int_{\mathbb{R}} |F^{(\tau-k)}(w - x - y)|^2 \rho(x) dx \right) < C_{F_w}^{(\tau-k)},$$

where $C_{F_w}^{(\tau-k)}$ is some positive constant.

By proposition 3, we know that $\left(\int_{\mathbb{R}} |H_{e_k}^\sigma(x)|^2 \rho(x) dx \right) = 1 < \infty$. With these analyses, we can then obtain the following:

$$\|F_i^{(\tau)}\|_{L^1(\mathbb{R})} \leq \sum_{k=0}^{\tau} \binom{\tau}{k} \frac{\sqrt{k!}}{\sigma^k} (C_{F_w}^{(\tau-k)})^{\frac{1}{2}} < \infty \quad (21)$$

Now we complete the first part of the proof.

For the L^2 norm, since $\int_{\mathbb{R}} |H_{e_k}^\sigma(x)|^2 \rho(x) dx = 1$, there must exist a supremum C_H such that $|H_{e_k}^\sigma(x)|^2 \rho(x) < C_H, \forall x \in \mathbb{R}$. Therefore, we can write the following:

$$\begin{aligned} \|F_i^{(m)}\|_{L^2(\mathbb{R})} &\leq \sum_{k=0}^m \binom{m}{k} \left(\int_{\mathbb{R}} \left| F^{(m-k)}(w-y-x) \frac{(-1)^k}{\sigma^k} \sqrt{k!} H_{e_k}^\sigma(x) \frac{1}{\sqrt{2\pi\sigma^2}} e^{-\frac{x^2}{2\sigma^2}} \right|^2 dx \right)^{\frac{1}{2}} \\ &\leq \sum_{k=0}^m \binom{m}{k} \left(C_H \frac{k!}{\sigma^{2k}} \int_{\mathbb{R}} |F^{(m-k)}(w-y-x)|^2 \rho(x) dx \right)^{\frac{1}{2}} \\ &< \sum_{k=0}^m \binom{m}{k} \left(C_H \frac{k!}{\sigma^{2k}} C_{F_w}^{(m-k)} \right)^{\frac{1}{2}} < \infty \end{aligned}$$

For the infinity norm, we denote $e^{\frac{(1-\epsilon)x^2}{2\sigma^2}} = \rho(x)^{\epsilon-1}$. Note that $H_{e_k}^\sigma(x)$ is a k -th order polynomial, i.e., the asymptotic behavior of $H_{e_k}^\sigma(x)$ is $O(x^k)$. We first establish that there exists a finite supremum $C_H^{\epsilon_1}$ for the product $F_H(x) := H_{e_k}^\sigma(x) \rho^{\epsilon_1}(x)$, where $\epsilon_1 > 0$ and $x \in \mathbb{R}$.

Since $\rho(x) = \frac{1}{\sqrt{2\pi\sigma^2}} e^{-\frac{x^2}{2\sigma^2}}$, for any $\epsilon_1 > 0$, $\rho(x)$ decays exponentially as $x \rightarrow \pm\infty$, while $H_{e_k}^\sigma(x)$, as a polynomial, can increase or decrease at most polynomially in x . Therefore, the product $F_H(x)$ exhibits a finite bound as $x \rightarrow \pm\infty$.

Furthermore, for any sufficiently large but finite interval $[a, b]$, $F_H(x)$ is continuous by construction. By applying the extreme value theorem, we conclude that it attains finite upper and lower bounds on any such interval. Now consider $G_W(x) := F^{(\tau)}(w-y-x) \rho^{\epsilon_2}(x)$, where $\epsilon_2 > 0$ and w, y are constants. Similar to the previous case, we examine the behavior of $G_W(x)$ as $x \rightarrow \pm\infty$.

From the analysis in proposition 1, we know that $F \in C^m(\mathbb{R})$ with at most polynomial growth. This means that for each $k = 0, 1, \dots, m$, there exist constants $C_k, p_k > 0$ such that $|F^{(k)}(x)| \leq C_k(1 + |x|^{p_k})$ for all $x \in \mathbb{R}$. When combined with the exponential decay of $\rho^{\epsilon_2}(x)$, the product $G_W(x) := F^{(\tau)}(w-y-x) \rho^{\epsilon_2}(x)$ decays rapidly enough to ensure a finite supremum. This is because for any polynomial growth of $F^{(\tau)}$, the exponential decay of ρ^{ϵ_2} will dominate as $|x| \rightarrow \infty$. By applying dominated convergence properties, we establish that $G_W(x)$ has a finite supremum, denoted $C_{F_w}^{\epsilon_2}$, for any given $\epsilon_2 > 0$ and derivative order τ .

Thus, we conclude that for the supremum norm:

$$\sup_{\substack{x \in \mathbb{R} \\ \tau \in \{0, \dots, m-1\}}} \left| e^{(1-\epsilon)\frac{x^2}{2\sigma^2}} F_i^{(\tau)}(x) \right|$$

we have:

$$\begin{aligned} &\left\| e^{(1-\epsilon)\frac{x^2}{2\sigma^2}} F_i^{(\tau)}(x) \right\|_{L^\infty(\mathbb{R})} \\ &\leq \sum_{k=0}^{\tau} \binom{\tau}{k} \left\| \rho(x)^{\epsilon-1} F^{(\tau-k)}(w-y-x) \rho^{(k)}(x) \right\|_{L^\infty(\mathbb{R})} \\ &= \sum_{k=0}^{\tau} \binom{\tau}{k} \left\| \rho(x)^{\epsilon-1} F^{(\tau-k)}(w-y-x) \rho(x) H_{e_k}^\sigma(x) \frac{(-1)^k \sqrt{k!}}{\sigma^k} \right\|_{L^\infty(\mathbb{R})} \\ &\leq \sum_{k=0}^{\tau} \binom{\tau}{k} \left\| \rho(x)^{\frac{\epsilon}{2}} F^{(\tau-k)}(w-y-x) \right\|_{L^\infty(\mathbb{R})} \left\| H_{e_k}^\sigma(x) \frac{(-1)^k \sqrt{k!}}{\sigma^k} \rho(x)^{\frac{\epsilon}{2}} \right\|_{L^\infty(\mathbb{R})} \\ &\leq \sum_{k=0}^{\tau} \binom{\tau}{k} C_H^{\frac{\epsilon}{2}} \frac{\sqrt{k!}}{\sigma^k} C_{F_w}^{\frac{\epsilon}{2}(\tau-k)} \end{aligned}$$

By construction, we need choose $\epsilon \in (\max\{0, 1 - \sigma^2\}, 1)$. In the last inequality, we obtain the supremum by setting $\epsilon_1 = \epsilon_2 = \frac{\epsilon}{2}$. Since $\tau \in [0, m - 1]$ is finite, the finite summation of bounded values is finite, thus giving

$$\sup_{\substack{x \in \mathbb{R} \\ \tau \in \{0, \dots, m-1\}}} \left| e^{(1-\epsilon)\frac{x^2}{2\sigma^2}} F_i^{(\tau)}(x) \right| < \infty.$$

Application of Theorem: With the above lemma established, we now apply the results from [Kazashi et al., 2023], Proposition 4.2, to our numerical setup in the Bass-LV model.

Theorem (Kazashi 2023, Proposition 4.2): Let $m \in \mathbb{N}$ represent the smoothness order of the function g . Assume that $g^{(\tau)} : \mathbb{R} \rightarrow \mathbb{R}$ is absolutely continuous on any compact interval for each derivative order $\tau = 0, \dots, m - 1$, and that the m -th derivative, $g^{(m)}$, belongs to the space $L^2(\mathbb{R})$ (the space of square-integrable functions). Additionally, g must satisfy the following two conditions:

1. **Local Regularity:** The m -th order Sobolev norm of g , denoted as $\|g\|_m^*$, is uniformly bounded over all compact intervals $I \subset \mathbb{R}$. This norm is defined as:

$$\|g\|_m^* := \sup_{\substack{I \subset \mathbb{R} \\ |I| < \infty}} \|g\|_{m,I} := \sup_{\substack{I \subset \mathbb{R} \\ |I| < \infty}} \left(\sum_{\tau=0}^{m-1} \left(\int_I g^{(\tau)}(x) dx \right)^2 + \int_I |g^{(m)}(x)|^2 dx \right)^{1/2}.$$

This norm ensures that g and its derivatives up to order m are well-behaved over compact intervals.

2. **Decay at Infinity:** The function g must exhibit a controlled decay at infinity, expressed as:

$$\|g\|_{m,\text{decay}} := \sup_{\substack{x \in \mathbb{R} \\ \tau \in \{0, \dots, m-1\}}} \left| e^{(1-\epsilon)\frac{x^2}{2}} g^{(\tau)}(x) \right| < \infty, \quad \text{for some } \epsilon \in (0, 1).$$

This condition ensures that $g(x)$ and its derivatives decay rapidly enough as $x \rightarrow \pm\infty$, governed by the exponential decay factor $e^{(1-\epsilon)\frac{x^2}{2}}$.

Given these assumptions, the error for the n -point Trapezoidal Rule Scheme $Q_{n,T}^*(g)$ with a cutoff interval $[-T, T]$ is bounded by:

$$\left| \int_{\mathbb{R}} g(x) dx - Q_{n,T}^*(g) \right| \leq C (\|g\|_m^* + \|g\|_{m,\text{decay}}) \frac{(\ln n)^{m/2+1/4}}{n^m},$$

where C is a constant independent of n and g , but dependent on m and ϵ . Here, the Trapezoidal Rule approximation $Q_{n,T}^*(g)$ is given by:

$$Q_{n,T}^*(g) := \frac{2T}{n} \sum_{j=0}^{n-1} g(\xi_j^*),$$

where $\xi_j^* := \frac{2T}{n}j - T$, and $T = \sqrt{\frac{2}{(1-\epsilon)}m \ln n}$ is the cutoff interval.

Adaptation for Bass-LV Model: In the Bass-LV implementation, we modify the theorem to match the specifics of our integrand $g(x)$, which is given by:

$$g(x) = F(w - y - x) \cdot \rho(x),$$

where $\rho(x) = \frac{1}{\sqrt{2\pi\sigma^2}} e^{-\frac{x^2}{2\sigma^2}}$ is the weighted function representing the heat kernel. The prerequisite for $g(x)$ is satisfied in our proof above, the parameters w and y are constants, and $F(w - y - x)$ is the piecewise polynomial representation of the distribution function obtained in each iteration, which upon convergence of the algorithm, yields the final distribution $F_{W_{T_i}}$.

We set $T = Nh$, $n = 2N + 1 \geq 2$, and $h = \frac{2T}{n}$, where N is the number of quadrature points used. The term $1 - \epsilon$ is adjusted to reflect the variance in the heat kernel, given by:

$$1 - \epsilon = \frac{1 - \epsilon}{\sigma^2}, \quad \epsilon \in (\max\{1 - \sigma^2, 0\}, 1),$$

where $\sigma^2 = T_{i+1} - T_i$ represents the time interval between maturities T_i and T_{i+1} .

Applying these modifications, we derive the optimal parameter settings for the Trapezoidal Rule Scheme for the inner integrand as follows:

$$Nh = \sqrt{\frac{2(T_{i+1} - T_i)}{(1 - \epsilon)} m \ln(2N + 1)}, \quad h = \frac{\sqrt{\frac{2(T_{i+1} - T_i)}{(1 - \epsilon)} m \ln(2N + 1)}}{N}.$$

Outer Integrand: The outer integrand, $F_{\mu_{i+1}}^{-1}$, is represented by a finite-order smoothness spline interpolation. Since the inputs to this function are also finite, similar results for optimality can be applied to the outer integrand, by imposing its own smoothness order and choosing ϵ independently within the interval $\epsilon \in (\max\{1 - \sigma^2, 0\}, 1)$.

Convergence Rate: From the results above, we conclude that the convergence rate of the Trapezoidal Rule Scheme for a single integrand in the Bass-LV implementation is:

$$\mathcal{O}\left(\frac{(\ln n)^{m/2+1/4}}{n^m}\right),$$

where m is the smoothness order of the integrand, and n represents the number of points counted in the Trapezoidal Rule.

Disclaimer

This paper was prepared for informational purposes in part by the Quantitative Research Group of JPMorgan Chase & Co. This paper is not a product of the Research Department of JPMorgan Chase & Co. or its affiliates. Neither JPMorgan Chase & Co. nor any of its affiliates makes any explicit or implied representation or warranty and none of them accept any liability in connection with this paper, including, without limitation, with respect to the completeness, accuracy, or reliability of the information contained herein and the potential legal, compliance, tax, or accounting effects thereof. This document is not intended as investment research or investment advice, or as a recommendation, offer, or solicitation for the purchase or sale of any security, financial instrument, financial product or service, or to be used in any way for evaluating the merits of participating in any transaction.

References

- Antoine Conze and Pierre Henry-Labordere. Bass construction with multi-marginals: Lightspeed computation in a new local volatility model. *Available at SSRN 3853085*, 2021. doi:10.2139/ssrn.3853085.
- Bruno Dupire et al. Pricing with a smile. *Risk*, 7(1):18–20, 1994.
- Emanuel Derman, Iraj Kani, and Joseph Z Zou. The local volatility surface: Unlocking the information in index option prices. *Financial analysts journal*, 52(4):25–36, 1996.
- Thomas F Coleman, Yuying Li, and Arun Verma. Reconstructing the unknown local volatility function. In *Quantitative Analysis In Financial Markets: Collected Papers of the New York University Mathematical Finance Seminar (Volume II)*, pages 192–215. World Scientific, 2001.
- Mohamed Bouzoubaa and Adel Osseiran. *Exotic options and hybrids: A guide to structuring, pricing and trading*. John Wiley & Sons, 2010. doi:10.1002/9781119206965.
- Antonie Kotzé, Rudolf Oosthuizen, and Edson Pindza. Implied and local volatility surfaces for south african index and foreign exchange options. *Journal of Risk and Financial Management*, 8(1):43–82, 2015. doi:10.3390/jrfm8010043.
- Julio Backhoff, Mathias Beiglböck, Martin Huesmann, and Sigrid Källblad. Martingale benamou–brenier: a probabilistic perspective. *arXiv preprint arXiv:1708.04869*, 2017. doi:10.48550/arXiv.1708.04869.
- Beatrice Acciaio, Antonio Marini, and Gudmund Pammer. Calibration of the bass local volatility model. *arXiv preprint arXiv:2311.14567*, 2023. doi:10.48550/arXiv.2311.14567.
- Bertram Tschiderer. q -bass martingales. *arXiv preprint arXiv:2402.05669*, 2024. doi:10.48550/arXiv.2402.05669.
- Gregoire Loeper. The measure preserving martingale sinkhorn algorithm. *arXiv preprint arXiv:2310.13797*, 2023. doi:10.48550/arXiv.2310.13797.
- Julio Backhoff-Veraguas, Walter Schachermayer, and Bertram Tschiderer. The bass functional of martingale transport. *arXiv preprint arXiv:2309.11181*, 2023a. doi:10.48550/arXiv.2309.11181.
- Julio Backhoff-Veraguas, Mathias Beiglböck, Walter Schachermayer, and Bertram Tschiderer. The structure of martingale benamou brenier in r^d . *arXiv preprint arXiv:2306.11019*, 2023b. doi:10.48550/arXiv.2306.11019.
- Gaspard Monge. Mémoire sur la théorie des déblais et des remblais. *Mem. Math. Phys. Acad. Royale Sci.*, pages 666–704, 1781.
- Pierre Henry-Labordere. From (martingale) schrodinger bridges to a new class of stochastic volatility model. *Available at SSRN 3353270*, 2019a. doi:10.2139/ssrn.3353270.
- Hadrien De March and Pierre Henry-Labordere. Building arbitrage-free implied volatility: Sinkhorn’s algorithm and variants. *arXiv preprint arXiv:1902.04456*, 2019. doi:10.48550/arXiv.1902.04456.

- Stephan Eckstein and Michael Kupper. Computation of optimal transport and related hedging problems via penalization and neural networks. *Applied Mathematics & Optimization*, 83(2):639–667, 2021.
- Pierre Henry-Labordere. (martingale) optimal transport and anomaly detection with neural networks: A primal-dual algorithm. *arXiv preprint arXiv:1904.04546*, 2019b. doi:10.48550/arXiv.1904.04546.
- David Hobson and Anthony Neuberger. Robust bounds for forward start options. *Mathematical Finance: An International Journal of Mathematics, Statistics and Financial Economics*, 22(1):31–56, 2012.
- Mathias Beiglböck, Pierre Henry-Labordere, and Friedrich Penkner. Model-independent bounds for option prices—a mass transport approach. *Finance and Stochastics*, 17:477–501, 2013.
- Yan Dolinsky and H Mete Soner. Martingale optimal transport and robust hedging in continuous time. *Probability Theory and Related Fields*, 160(1):391–427, 2014. doi:10.1007/s00440-013-0531-y.
- Pierre Henry-Labordère and Nizar Touzi. An explicit martingale version of the one-dimensional brenier theorem. *Finance and Stochastics*, 20:635–668, 2016.
- Ivan Guo, Grégoire Loeper, and Shiyi Wang. Local volatility calibration by optimal transport. *arXiv preprint arXiv:1709.08075*, 2017. doi:10.48550/arXiv.1709.08075.
- Pierre Henry-Labordère. *Model-free hedging: A martingale optimal transport viewpoint*. Chapman and Hall/CRC, 2017.
- Marcel Nutz, Johannes Wiesel, and Long Zhao. Martingale schrödinger bridges and optimal semistatic portfolios. *Finance and Stochastics*, 27(1):233–254, 2023.
- Michal Benko, Matthias Fengler, Wolfgang Härdle, and Milos Kopa. On extracting information implied in options. *Computational statistics*, 22:543–553, 2007. doi:10.1007/s00180-007-0061-0.
- Bernhard Brunner and Reinhold Hafner. Arbitrage-free estimation of the risk-neutral density from the implied volatility smile. *Journal of Computational Finance*, 7(1):75–106, 2003.
- Matthias R Fengler and Lin-Yee Hin. A simple and general approach to fitting the discount curve under no-arbitrage constraints. *Finance research letters*, 15:78–84, 2015.
- Yoshihito Kazashi, Yuya Suzuki, and Takashi Goda. Suboptimality of gauss–hermite quadrature and optimality of the trapezoidal rule for functions with finite smoothness. *SIAM Journal on Numerical Analysis*, 61(3):1426–1448, 2023. doi:10.1137/22m1480276.
- Jim Gatheral and Antoine Jacquier. Arbitrage-free svi volatility surfaces. *Quantitative Finance*, 14(1):59–71, 2014. doi:10.1080/14697688.2013.819986.
- Justin Birru and Stephen Figlewski. The impact of the federal reserve’s interest rate target announcement on stock prices: A closer look at how the market impounds new information. *Script. New York University Stren School of Business*, 2010.
- Lykourgos Alexiou, Amit Goyal, Alexandros Kostakis, and Leonidas Rompolis. Pricing event risk: Evidence from concave implied volatility curves. *Swiss Finance Institute Research Paper*, (21-48), 2023. doi:10.1093/rof/rfaf016.
- G Mastroianni and Giovanni Monegato. Error estimates for gauss-laguerre and gauss-hermite quadrature formulas. In *Approximation and Computation: A Festschrift in Honor of Walter Gautschi: Proceedings of the Purdue Conference, December 2–5, 1993*, pages 421–434. Springer, 1994. doi:10.1007/978-1-4684-7415-2_28.